Heat flow and surface hydrocarbons on the Brunei continental margin

Gary W. Zielinski, Malvin Bjorøy, Robyn L. B. Zielinski, and Ian L. Ferriday

ABSTRACT

Simultaneous heat flow and geochemical gravity coring data from 186 sites on the Brunei margin reveal abundant thermogenic hydrocarbons in the landward half of our study area, where the mean heat flow is 83.7 ± 66.5 mW/m^2. Seaward, the mean heat flow is 59.0 ± 22.6 mW/m^2, and surface thermogenic hydrocarbons are largely absent. In accord with active accretionary complexes, the low-heat-flow zone coincides with the Palawan (northwest Borneo, Nansha) Trough paleosubduction zone. The high-heat-flow zone of hydrothermal convection and hydrocarbon seepage coincides with the landward, land-derived Baram delta sediments, constituting a pseudo–accretionary prism. The transition from oil to gas production with increasing geothermal gradient, observed in well data, appears to be reflected in our surface data. Equality of Brunei and China margin heat flow predicts a common thermotectonic origin that predates by less than or equal to 5 m.y., the oldest (32 Ma) magnetic lineations in the South China Sea Basin. Thermal effects of prior active subduction, if any, have dissipated, and Brunei margin heat flow has rebounded to theoretical passive-margin values.

A single megaseep exhibits maximum heat flow (604 mW/m^2) coincident with anomalous thermogenic hydrocarbons. Vertical fluid flow at 1.7 cm/yr (0.67 in./yr) (5.5×10^{-10} m/s; 1.80×10^{-11} ft/s) from 6 km (3.7 mi) depth, implying greater than 30 times focusing of flow, can account for this heat flow and provide hydrocarbon transport from potential sources. A 42 times higher flow rate via bubble ascent or continuous gas-phase flow can also account for our data. Simple models of fluid flow around fault-bounded sediment troughs reproduce the observed heat flow. These models predict that measurements confined to trough interiors, where heat flow is uniform, seriously underestimate mean regional heat flow (23–80%) and thermal maturation; whereas heat flow at all geochemical coring sites yields reliable means.

Manuscript received October 12, 2006; provisional acceptance November 2, 2006; revised manuscript received December 7, 2006; final acceptance January 15, 2007.
DOI:10.1306/01150706117

AUTHORS

GARY W. ZIELINSKI ~ *Omegalink International, Ltd., 2382 Rt. 118, Dorchester, New Hampshire 03266; omegalink@juno.com*

Gary holds a Ph.D. from Columbia University under M. G. Langseth (Heat Flow Department), Lamont-Doherty Earth Observatory. He spent 6 years at Gulf Research and Development (Harmarville Lab), where he studied measurement and modeling of hydrocarbon thermal regimes. He continued this work at Brookhaven National Laboratory as visiting research associate at Lamont-Doherty and (1989–present) as a director at Omegalink International Ltd.

MALVIN BJORØY ~ *Surface Geochemical Services AS, P.O. Box 5740, 7437 Trondheim, Norway; malvin@geolabnor.no*

Malvin Bjorøy, a graduate of organic chemistry from the University of Bergen, spent 8 years at the Norwegian Continental Shelf Institute, where he established the surface geochemistry group and became head of the department, establishing Geolab Nor AS in 1985. Malvin has directed more than 70 surface geochemical surveys, mainly in the Norwegian, North, and Barents Seas and in the Far East. Malvin has published more than 80 articles in international journals.

ROBYN L. B. ZIELINSKI ~ *Omegalink International, Ltd., 2382 Rt. 118, Dorchester, New Hampshire 03266; omegalink@juno.com*

Robyn holds a B.S. degree from the Virginia Polytechnic Institute and State University, with graduate studies at Virginia Commonwealth University. She began working with Omegalink International, Ltd., in 1980 and has since participated in numerous marine and land-based heat-flow and geochemical data acquisition programs. This includes data reporting and publication in international journals. Robyn currently serves Omegalink as a director specializing in field operations.

IAN L. FERRIDAY ~ *Geolab Nor AS, P.O. Box 5740, 7437 Trondheim, Norway; iafe@geolabnor.no*

Ian is a graduate of geology from Imperial College, London, United Kingdom. Besides routine well geochemistry and visual kerogen microscopy, Ian's work has included numerous regional well projects and surface geochemical

surveys worldwide. Ian is currently laboratory manager at Geolab Nor AS, Trondheim, Norway, having been involved with more than 20 articles in international journals.

ACKNOWLEDGEMENTS

We thank the Petroleum Unit of Brunei for permission to publish these data results. We thank the captain and crew of the M/V *Seaway Pioneer*, and we thank E. Bonazza, J. Heath, S. Kirkeby, and S. Seehuus for shipboard support. We thank W. Van Steveninck and W. Zielinski for engineering and quality control support. We thank M. Abrams, J. Curiale, R. Hatton, R. Sassen, and R. Von Herzen for valuable comments and reviews of earlier versions of this work. We especially thank *AAPG Bulletin* reviewers B. Katz and D. Schumacher for reviews that led to further improvement and AAPG editor E. Mancini and geology consultant F. Whitehurst for helpful suggestions. This article elaborates on an AAPG poster session (Zielinski et al., 2003). We dedicate this article to Marcus G. Langseth.

Megaseep data reveal systematic changes in thermogenic hydrocarbons and heat flow with distance from the seep axis. A simple diffusion model represents these changes in terms of bulk near-surface processes. A simple thermogenic model also simulates gas data; however, thermal-maturation parameters indicate no causal connection between megaseep heat flow and thermogenesis. Invariant parameters, less affected by migration, fractionation, mixing, and biodegradation, remain anomalous more than 250 m (800 ft) from the megaseep axis, encompassing all four high-heat-flow sites. This constitutes a significantly greater aperture for identifying seeps in coring data compared with headspace gases, found anomalous at one site only. Like heat flow, invariant parameters that are extreme at the megaseep may particularly reflect more active seepage, where hydrocarbons are less altered and more closely reflect their sources. Regional data covering 10,000 km^2 (3600 mi^2) largely reflect the same near-surface processes occurring within 500 m (1600 ft) of the megaseep. Consequently, distances from regional seeps and paleoheat flow can be inferred.

INTRODUCTION

Models based on the kinetics of kerogen degradation (Tissot and Espitalie, 1975) led to the integration of heat flow and petroleum geochemistry (e.g., Tissot and Welte, 1978; MacKenzie and McKenzie, 1983) that largely focused on hydrocarbon maturation and generation for now-traditional basin analysis (e.g., Lerche, 1990). The fluid-flow implications of secondary migration and its effect on the thermal field (e.g., Fowler, 1980; Roberts, 1981) provided another application for heat flow (e.g., Zielinski and Bruchhausen, 1983; Zielinski et al., 1985). Renewed interest in surface hydrocarbon geochemistry (Jones and Drozd, 1983; Schumacher and Abrams, 1996) resulted in land-based thermal measurements performed at the same sites sampled for geochemistry (Zielinski et al., 1985). We report results from successful simultaneous geochemical coring and marine heat-flow measurements (Appendix 1) conducted in 2 weeks in 2001. Resulting data represent 186 sites in water depths from 800 to 2700 m (2600 to 8800 ft) within a 10,000-km^2 (3600-mi^2) study area on the Brunei continental margin of the South China Sea (Figure 1). We use these data to investigate the global correlation between hydrocarbons and their thermal regimes (e.g., Klemme, 1975; Fowler, 1980; Zielinski and Bruchhausen, 1983; Zielinski et al., 1990; Nagihara et al., 2002; Ruppel et al., 2005).

Reliable correlation of thermogenic hydrocarbons with their sources is dependent on the knowledge of their evolution subsequent to seepage. Direct evidence for this derives from diverse studies (e.g., Bernard et al., 1977; Brooks et al., 1979; Abrams, 1996a, b; Sassen et al., 2003, 2004); however, data commonly represent a limited range of hydrocarbon parameters. A quantitative, chemically

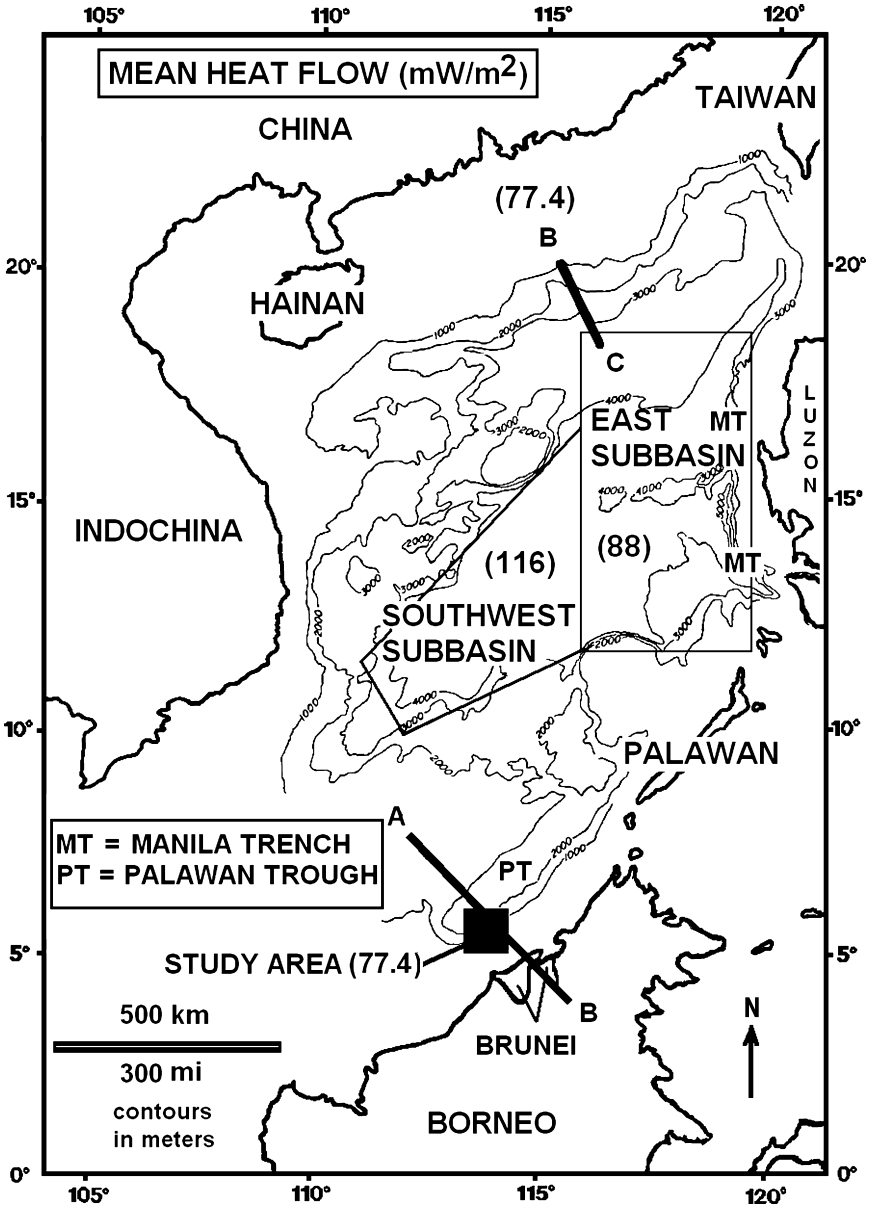

Figure 1. Study area, offshore Brunei and the South China Sea basins and margins (after Ru and Pigott, 1986). Line AB indicates the generalized location represented by Figure 2. Line BC approximately locates the Xia et al. (1995) China margin heat-flow data. Mean heat flow (mW/m^2) in parentheses.

independent indicator of seepage is commonly lacking or limited to direct observations of bubbles and chemosynthetic communities. In this study, sensitive, independent, quantitative evidence for active seepage is provided by the Ewing technique marine heat-flow measurements (Langseth, 1965) (Appendix 1) and a broad spectrum of hydrocarbon parameters. The purpose of this article is to report the preliminary results of this unique data set and its implication to surface geochemical data interpretation. We do so by focusing on seven megaseep data sites where heat flow and surface hydrocarbons are locally well constrained, and their relation to 179 regional sites.

GEOTHERMAL RESULTS

Heat-flow measurements at 186 sites reveal a mean heat flow and standard deviation of 77.6 ± 59.8 mW/m^2 for our survey area (Figure 1). This compares favorably with the value for marginal seas of 76.5 mW/m^2 (Lee and Uyeda, 1965); however, our data show greater than 30% higher standard deviation. Nearby, Tertiary back-arc basins exhibit high mean heat flow (~90 mW/m^2), but with a low standard deviation of 13.0 mW/m^2 (Watanabe et al., 1977). Our Brunei heat flow and standard deviation are comparable to the 79.4 ± 61.8 mW/m^2 reported for ocean ridges (Lee,

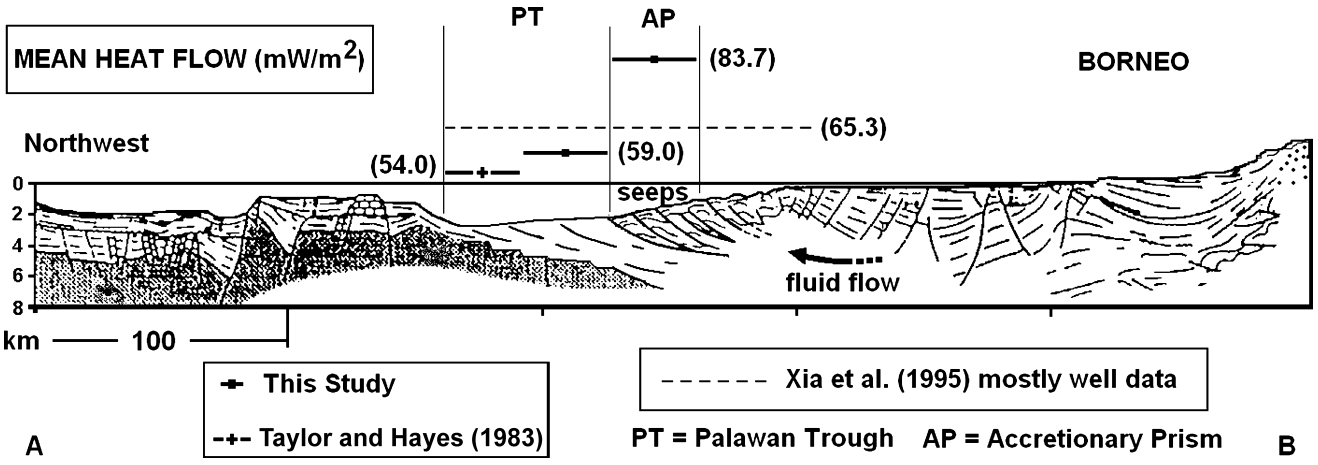

Figure 2. Cross section (AB, Figure 1) through our study area illustrating the long-held paleosubduction zone model of the Palawan (also known as northwest Borneo or Nansha) Trough (PT) and accretionary prism (AP) (modified after Letouzey et al., 1988; Blanche and Blanche, 1997). Mean heat flow increases slightly from deeper to shallower in the trough (PT), and then significantly increases over the landward prism (AP) caused by the hypothesized fluid flow (arrow) and concomitant seepage of observed hydrocarbons. Data for this study are the means for the landward and seaward zones in Figure 4. Mostly from well data (Xia et al., 1995), the mean heat flow for the broader Palawan (Nansha) Trough (dashed line) equals the average of the three shallow-probe means.

1970), where the high standard deviation is now widely accepted to result from hydrothermal circulation (e.g., Pollack et al., 1993). The earliest global heat-flow compilations (e.g., Lee, 1970) reveal a similarly high standard deviation associated with continental margins as well.

Our study area on the Brunei margin lies within what has long been interpreted as the paleosubduction zone of the Palawan (also known as northwest Borneo or Nansha) Trough and associated accretionary prism (Figure 2). Hutchison (2005) argues against the accretionary prism interpretation, stressing that the associated sediments are derived from mainland Borneo, not from a subducting plate. However, he also compares the evolution of the region with that of the active Barbados Ridge complex. His cross sections show a decollement descending beneath the Baram delta sediments. Faulting appears similar to that within the accretionary prism in Figure 2, but resulting from delta deposition and not compressional tectonics. Our highly varying heat flow is also consistent with the heat- and fluid-flow regimes of active accretionary complexes (Langseth and Moore, 1990; Langseth et al., 1990; Langseth and Silver, 1996; Ruppel and Kinoshita, 2000), where active fluid flow predominates within accretionary prisms, but not with their generally low mean heat flow believed to be associated with active subduction. Hence, in terms of fluid flow, the land-derived sediments of the Baram delta constitute a pseudo–accretionary prism. Xia et al. (1995) report a mean heat flow of 65.3 ± 18.0 mW/m^2 and no low-heat-flow belt for the broad Palawan Trough (Figure 1), based largely on well data (dashed line, Figure 2). They contrast this with the reported 40% lower heat flow (39.0 ± 17.3 mW/m^2) caused by the active subduction of cold oceanic crust along the Manila Trench (MT, Figure 1). Likewise, our higher mean heat flow implies that thermal effects of past subduction, if any, have largely decayed in the 16 m.y. since the end of sea-floor spreading in the South China Sea Basin (Taylor and Hayes, 1983). This 16 m.y. is equivalent to one thermal time constant for the 40-km (25-mi)-thick oceanic crust estimated by Furukawa (1995).

Watanabe et al. (1977) report seven heat-flow measurements from the Palawan Trough. Two of these have low values, with one less than 21 mW/m^2, whereas our lowest measured heat flow is 15.2 mW/m^2. Such low individual values typically indicate hydrothermal circulation (Williams et al., 1974; Pollack et al., 1993). For the South China Sea Basin (Figure 1), high mean heat flow is reported for the northern East subbasin (~88 ± 10 mW/m^2) and the Southwest subbasin (~116 ± 18 mW/m^2) (Watanabe et al., 1977; Xia et al., 1995; Blanche and Blanche, 1997). Our Brunei mean agrees with the 77.4 ± 10.5 mW/m^2 reported for the northern margin of the South China Sea Basin, based on 47 measurements (Xia et al., 1995) along line BC in Figure 1. However, the high standard deviation of our Brunei data and its postulated hydrothermal cause are absent in these other locations. Based on 39 measurements in the Zengmu (Sarawak) Basin adjacent

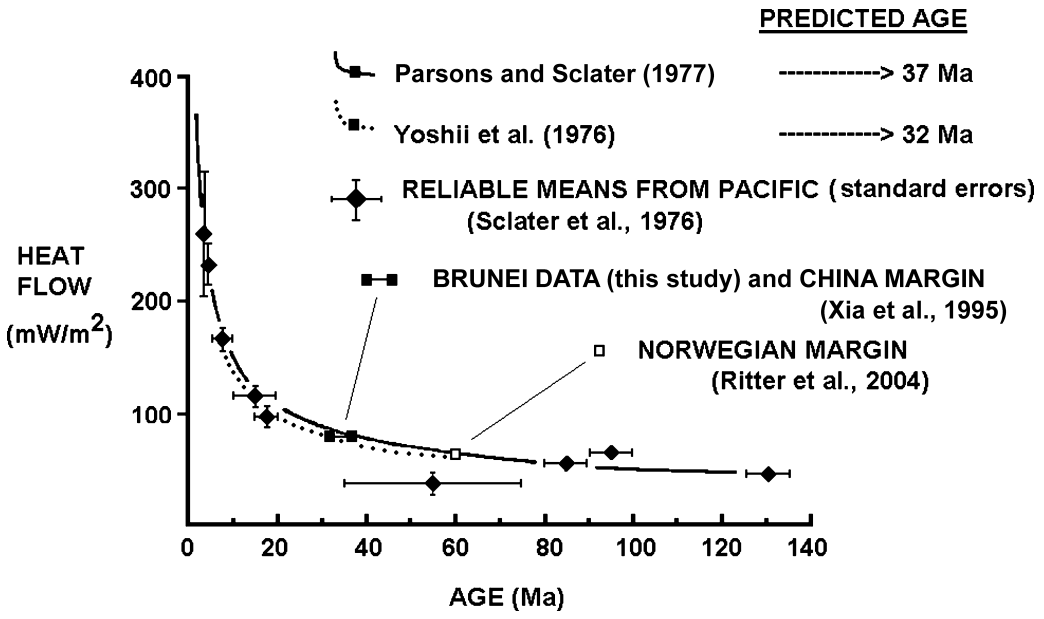

Figure 3. The global Parsons and Sclater (1977) heat flow versus age relation (solid curve) and reliable heat-flow means (solid diamonds) and standard errors for the Pacific Ocean basin. Nearly equal mean heat flow predicts a common age of 37 Ma for the present study (solid squares) and for the China margin (BC, Figure 1); however, models predicting more rapid cooling (e.g., Yoshii et al., 1976, dotted curve) reduce this estimate to about 32 Ma. Data from the 60-Ma Norwegian passive margin (open square) and for this study have equal standard error (4.4 mW/m^2).

(south and west) to our study area, high and moderately variable heat flow (97.1 ± 25.7 mW/m^2) is attributed to magmatic and hydrothermal activity associated with Tertiary extension (Xia et al., 1995).

Anderson (1980) showed that several marginal basins in the western Pacific conform to the global heat flow-versus-age relation of Parsons and Sclater (1977). Taylor and Hayes (1983) confirmed this relationship by correlating heat-flow measurements with marine magnetic lineations that date a middle Oligocene (32-Ma) onset of sea-floor spreading in the East subbasin (Figure 1). Based on higher heat flow (~116 ± 18 mW/m^2), Xia et al. (1995) ascribe a 10-m.y. lesser age to the Southwest subbasin. Applying the heat flow-age relation (solid curve, Figure 3) directly to our data (solid square) yields an age of 37 Ma for our Brunei margin survey area as well as for the continental slope of China (line BC, Figure 1). This implies that a single thermotectonic event at the Eocene–Oligocene boundary preceded sea-floor spreading (Taylor and Hayes, 1983) by 5 m.y., simultaneously affecting both northern and southern margins of the South China Sea Basin. However, Watanabe et al. (1977) compared their data to the Pacific Basin cooling model of Yoshii et al. (1976) (dotted curve, Figure 3), which predicts more rapid cooling than Parsons and Sclater (1977). More rapid cooling is also predicted for younger passive margins (Zielinski, 1977, 1979) relative to purely oceanic models because of 2-D heat transfer. Because the South China Sea region departs significantly from the Parsons and Sclater (1977) global depth-versus-age relation (Anderson, 1980; Taylor and Hayes, 1983; Xia et al., 1995), this criterion cannot give preference to either heat-flow model; neither can the heat-flow data (Ritter et al., 2004) from the early Tertiary (~60 Ma) passive Norwegian margin (open square, Figure 3) because both models (Yoshii et al., 1976; Parsons and Sclater, 1977) predict similar heat flow at that age. Compared with other published heat-flow data sets, both Ritter et al. (2004) and our Brunei data set are unique in consisting of hundreds of measurements performed in relatively small, individually isochronous areas. The resulting mean values are well controlled, having equal standard error(s) of 4.4 mW/m^2. For our data and for the China margin, Yoshii et al. (1976) (dotted curve, Figure 3) yield an age that agrees with the 32-Ma onset of sea-floor spreading (Taylor and Hayes, 1983) in the East subbasin (Figure 1). Based on our data results, more recent thermal events or sea-floor spreading (Ru and Pigott, 1986; Xia et al., 1995) do not affect heat flow on the Brunei or the China margins.

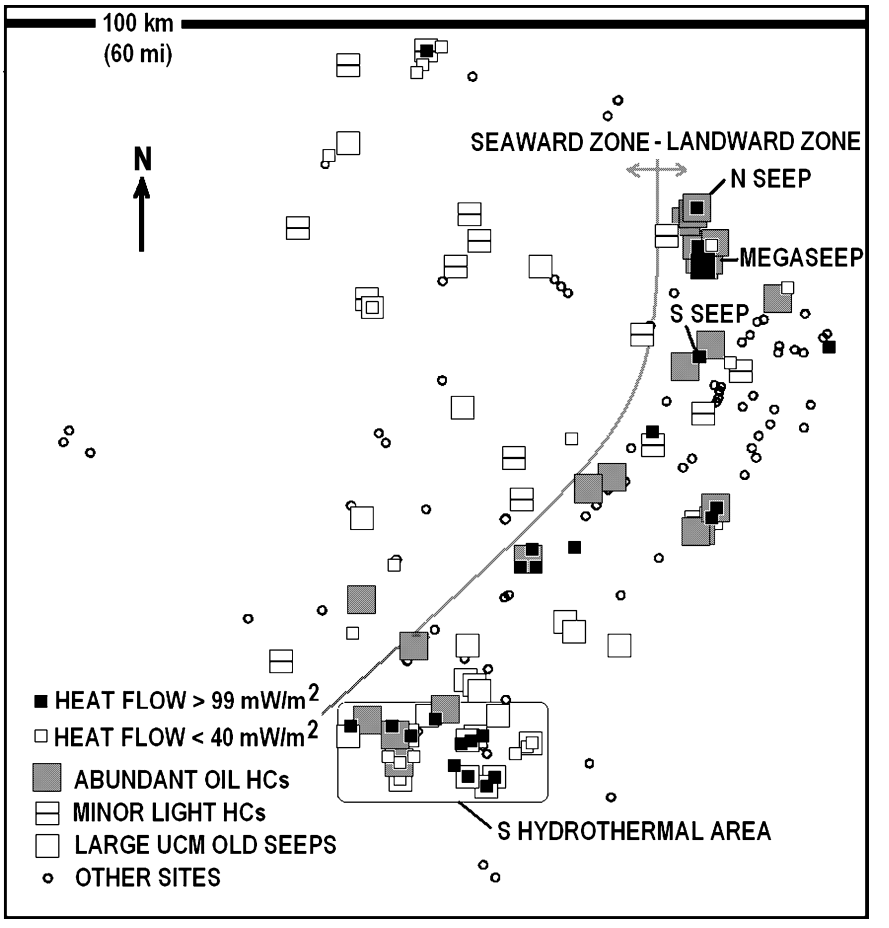

Figure 4. Anomalous heat flow (small squares) and sediment hydrocarbons (large squares) within our study area (Figure 1). The solid curve separates a landward high heat-flow (small solid squares) zone of abundant thermogenic hydrocarbons (large shaded squares) from a seaward low-heat-flow, geochemically quiescent zone. The seaward zone is associated with the Palawan Trough (PT) and the landward zone with the adjacent Baram delta pseudo–accretionary prism (AP) in Figure 2. The southern (S) hydrothermal area exhibits anomalous heat flow associated with recent seeps (large shaded squares) and biodegraded old seeps (large UCM, large open squares). UCM = unresolved complex mixture (e.g., Peters et al., 2005). Gas hydrates were observed only at the megaseep (604 mW/m^2) and northern (N) seep (241 mW/m^2). Abundant oil hydrocarbons indicate chromatograms (Appendix 1) with abundant n-alkanes, low carbon preference indices (CPI), and typical oil profiles with or without broad unresolved envelopes. Quantitative geochemical values are shown in Figures 7 –14. HC = hydrocarbon.

Langseth et al. (1990) applied the Parsons and Sclater (1977) heat flow-versus-age relationship to assess the effects of active subduction on the heat flow across the Barbados accretionary complex. Conversely, the accuracy of such models for Brunei margin age determination (solid squares, Figure 3) depends on the absence of significant subduction effects in our data. Our mean heat flow is 10 mW/m^2 (11.5%) lower than for the six (Taylor and Hayes, 1983) purely oceanic sites (87 ± 6 mW/m^2 at 30.5 ± 1.2 Ma) from the northern East subbasin (Figure 1) located 1000 km (600 mi) north of our study area. However, the mean for the adjacent China margin (line BC), with no history of subduction, is also lower by the same amount, and both are explained by ages and/or cooling rates in Figure 3. A significant subduction effect in our data implies a correspondingly significant difference in age between the southern margin and the purely passive northern margin of the South China Sea Basin, where subduction does not apply. Cooling plate model results in figure 10 of Carslaw and Jaeger (1959) predict greater than 90% decay of subduction effects on the geotherm (and heat flow) in t = 16 m.y. ($\kappa t/l^2 = 1$; $2l$ = 40 km; $\kappa = 0.8 \times 10^{-6}$ m^2/s). Based on the 26.3-mW/m^2 lower heat flow for the active Manila Trench versus the inactive Palawan (Nansha) Trough (Xia et al., 1995), we estimate maximum remaining subduction effect (if any) on our heat flow at less than 3 mW/m^2, and 2-D cooling would further lower this estimate.

Likewise, our lower mean heat flow compared with the 30-Ma Taylor and Hayes (1983) data cannot be attributed to sampling bias because of our program's site-specific (Abrams, 1996a) targeting of fluid-migration sites and seeps. If present, this bias results in erroneously higher mean heat flow, implying increased disparity between our data and those of Taylor and Hayes (1983) and Xia et al. (1995). Site-specific surveys may provide reliable sampling of the geothermal field in our study area because the seep targets are illusive, short-wavelength features, as evidenced by the many small open circles in Figure 4, where no anomalies (hydrocarbon or heat flow) were encountered.

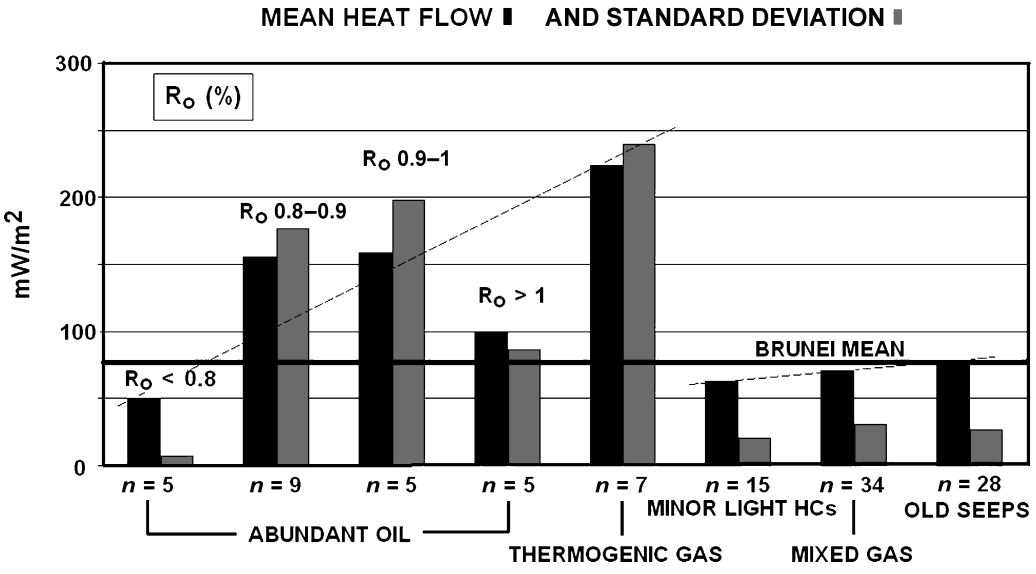

Figure 5. Heat-flow means (black) and standard deviations (gray) for the summary hydrocarbon groups. Trends (dashed lines) are speculative; however, only abundant oil and thermogenic gas hydrocarbon sites exhibit heat flow increasingly higher than the Brunei mean. Transition from oil to gas production with increasing geothermal gradient is seen in well data from the Palawan (Nansha) Trough (Xia et al., 1995). Values of R_o (%) are obtained from crossplots of steranes [$\%C_{29}\alpha\alpha 20S/(20S + 20R)$ versus $\%C_{29}\beta\beta/(\beta\beta + \alpha\alpha)$] and terpanes [$T_s/(T_s + T_m)$ versus $30d/(30d + 29\beta\alpha)$] where T_s and T_m are C_{27} hopanes, 18α-22,29,30-trisnorneohopane and 17α-22,29,30-trisnorhopane, 30d and 29βα are C_{30} diahopane and C_{29}βα-hopane (e.g., Peters et al., 2005), and by aromatic MPI (Radke et al., 1982; Radke and Welte, 1983; Radke, 1987). Abundant oil hydrocarbons indicate chromatograms (e.g., Appendix 1) with abundant n-alkanes, low carbon preference indices (CPI), and typical oil profiles with or without broad unresolved envelopes. Thermogenic gases exhibit high values of wetness, abundant branched and cyclic compounds, and low alkenes. Quantitative geochemical values are in Figures 7 –14.

HEAT FLOW AND HYDROCARBON DISTRIBUTION

Based on the amounts of C_{2+} n-alkanes and nonbiogenic associated compounds such as the branched and cyclic hydrocarbons, significant thermogenic hydrocarbons are present in the surface sediments of our study area. In addition to thermogenic light hydrocarbons, abundant oil and associated gas are present in the organic material (bitumen) extracted from sediments (e.g., Hunt, 1979; Waples, 1981). The magnitudes observed are represented by the chromatograms for anomalous seep sites (Appendix 1) and the crossplots of individual geochemical parameters (Appendix 4) to be discussed. The crossplots also allow comparison of seep data magnitudes with those for the entire data population. A large variation in the maturity of the liquid hydrocarbons is found in the samples, equivalent to R_o (vitrinite reflectance) of 0.6–1.3% (Figure 5). These values are obtained from crossplots of steranes [$\%C_{29}\alpha\alpha 20S/(20S + 20R)$ versus $\%C_{29}\beta\beta/(\beta\beta + \alpha\alpha)$] and terpanes [$T_s/(T_s + T_m)$ versus $30d/(30d + 29\beta\alpha)$], where T_s and T_m are C_{27} hopanes 18α-22,29,30-trisnorneohopane and 17α-22,29,30-trisnorhopane, 30d and 29βα are C_{30} diahopane and C_{29}βα-hopane (for general discussion and notation, see Peters et al., 2005), and from the aromatic methylphenanthrene index (MPI) (Radke et al., 1982; Radke and Welte, 1983; Radke, 1987). The distribution of heat-flow defined hot and cold spots is examined in relation to the summary hydrocarbon results for our study area in Figure 4. The data are separated into seaward and landward regions. The seaward, minor fraction of our data constitutes a relatively uniform low-heat-flow zone, where the mean heat flow is 59.0 ± 22.6 mW/m^2 and abundant oil-related hydrocarbons (large shaded squares) are largely absent. Landward, where the mean heat flow is 83.7 ± 66.5 mW/m^2, numerous hot (small solid squares) and cold (small open squares) spots occur in varying association with sites that frequently exhibit abundant oil-related hydrocarbons (large shaded squares). The indicated megaseep is where our two highest heat-flow values (509 and 604 mW/m^2) coexist with abundant thermogenic hydrocarbons, as does the third highest heat flow (241 mW/m^2) observed just north of the megaseep (N SEEP). Gas hydrates were observed in sediment cores from only these two seep

locations. The relative position of the two zones in our area (Figure 4) is consistent with prior observations of more variable and higher heat flow and fluid loss in accretionary prisms and uniformly lower heat flow found in the seaward subduction zones (e.g., Langseth and Moore, 1990). For our data (Figure 4), we associate the most significant hydrocarbon seepage and the high-heat-flow zone with the Palawan pseudo-accretionary prism (Baram delta) and the lack of observed seepage in the seaward zone of low heat flow with the adjacent Palawan Trough (Figure 2). In the south of the landward zone, a 15 × 30-km (9.3 × 18.6-mi) area (southern hydrothermal area, Figure 4) of very high and very low heat flow exists, where multiple sites are found to contain seeped hydrocarbons that are severely biodegraded (large unresolved complex mixture [UCM] values, large open squares) (e.g., Peters et al., 2005), suggesting these seeps to be presently inactive. Sample contamination, where it is in the form of UCM, commonly takes the form of a narrow (distillate-type) envelope with increased, although not commonly large, UCM values. Large and broad UCM (see chromatograms in Appendix 1) found in our study area (Figure 4) are more commonly associated with the degradation of seeped hydrocarbons. However, the highly variable heat flow in the southern hydrothermal area reflects active hydrothermal circulation, implying that the original source of hydrocarbons at depth has been depleted, its pathway to the surface interrupted, or seepage has shifted to adjacent nonbiodegraded (shaded) sites. Such transient seepage may be a product of the region's ongoing geohistory (Hutchison, 2005). The location of this area appears to coincide with the relatively high geothermal gradient reported by Xia et al. (1995).

The low-heat-flow, relatively hydrocarbon-void, seaward zone (Figure 4) represents 30% of all survey sites. In addition to being more numerous, a fraction of landward sites was selected using three-dimensional (3-D) seismic data acquired over only the landward zone. All other sites (landward and seaward) were selected beforehand using only two-dimensional (2-D) data, and reportedly, all 2-D generated landward sites survived any later 3-D seismic data scrutiny. Despite the size difference between the landward and seaward data sets, the respective success rates for encountering anomalous hydrocarbons (any of the three large squares, Figure 4) are about the same at 40%. Indeed, the more numerous landward sites include a proportionally greater number of background sites (small open circles, Figure 4), devoid of anomalous hydrocarbons or heat flow that were presumably added to the survey based on the 3-D seismic data. For our survey, this suggests that the advantage of 3-D over 2-D data for identifying site-specific targets is largely one of increased data coverage, and the seaward sites can be considered a population sample of the entire data set. However, only one seaward site (Figure 4) exhibits heat flow greater than 99 mW/m^2 (small solid squares) and only one separated seaward site exhibits abundant oil-associated hydrocarbons (large shaded squares), about 2% of all seaward sites. In significant contrast, 16% of landward sites exhibit abundant oil-associated hydrocarbons, and 20% exhibit high heat flow (small solid squares), with both frequently occurring at coinciding sites or in close proximity. The latter is further reflected in the mean heat-flow values for the sites of each of the summary hydrocarbon groups (Figure 5), where $R_o > 1\%$ data represent the most notable departure from speculative trends (dashed lines). However, only abundant oil and thermogenic gas hydrocarbon sites exhibit heat flow higher than the Brunei mean, and these overwhelmingly represent the landward zone in Figure 4. Xia et al. (1995) demonstrate an oil-window–like transition from oil production to gas production with increasing geothermal gradient based on well data from the broader Palawan (Nansha) Trough. This trend may be reflected in Figure 5 (left dashed line). The statistics support a significant difference between the landward and seaward zones, clearly shown by the areal separation of dark and light symbols in Figure 4 that is not caused by sampling bias.

Furthermore, our mean heat flow of 59.0 ± 22.6 mW/m^2 for the seaward zone corresponding to the Palawan Trough is in good agreement with a mean value of 54.0 ± 15.6 mW/m^2 for five measurements (Taylor and Hayes, 1983) from deeper in the trough (2305–2882 m; 7562–9455 ft) just north of our survey area (Figure 2). These measurements combined with ours indicate an increase in both heat flow and its standard deviation from the deep trough to the Palawan pseudo–accretionary prism (Baram delta), where the mean heat flow is 83.7 ± 66.5 mW/m^2 (Figure 2). To attribute this to sampling bias renders our seaward heat-flow data in disagreement with the adjacent (Taylor and Hayes, 1983) values. Furthermore, the Xia et al. (1995) value (65.3 ± 18.0 mW/m^2) for well data from the broad Palawan (Nansha) Trough falls between our two observed mean values (Figure 2) instead of significantly below the single mean value (83.7 mW/m^2) predicted if all of the observed difference between trough and landward sediments were caused by sampling bias. The average of our two heat-flow zones (71.3 mW/m^2)

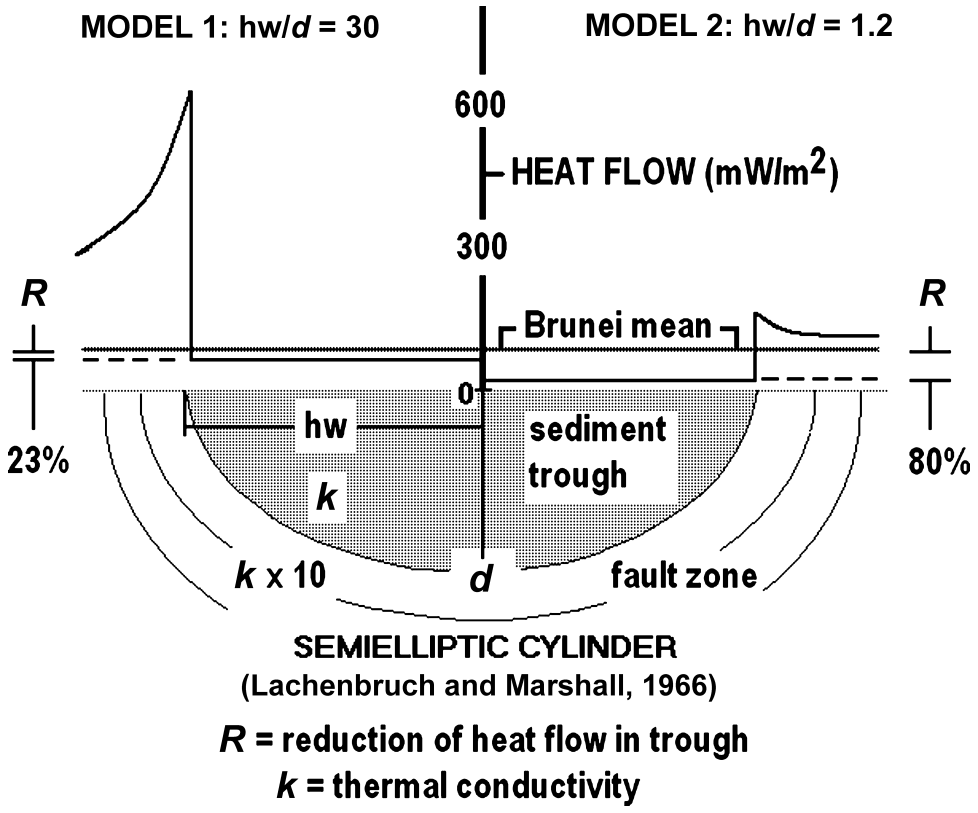

Figure 6. Theoretical heat flow (solid black curves and lines) across semielliptic cylinders of half-width–to–depth ratios (hw/*d*) of 30 (model 1, left) and 1.2 (model 2, right) for a constant heat flow of 77.6 mW/m^2 (Brunei mean) from depth. Inside the cylinder represents a sediment trough with thermal conductivity, *k,* and outside represents a faulted zone of convective heat transfer simulated by thermal conductivity $k \times 10$ ($K = 10$, Appendix 2). Models 1 and 2 reproduce our observed data range. Model 1 (left) also simulates the transition in heat flow from the Palawan Trough to the Baram delta pseudo–accretionary prism (PT-AP, Figure 2), represented by the model trough interior (59.7 mW/m^2) and the fault zone, respectively. The model 1 heat flow at the trough-fault zone boundary simulates high heat flow associated with decollements and observed at the megaseep. Theoretical heat flow across trough interiors is uniform but reduced significantly (*R*) below the Brunei mean.

is within 10% of the well data mean, and the average of all three means shown in Figure 2 (65.6 mW/m^2) essentially equals the well data mean (dashed line).

Fluid-Flow Models

Consistent with local geology, our range of heat-flow measurements can be simulated by a simple model of heat flow across a fault zone–bounded sediment trough (Figure 6). We treat the sediment trough as a 2-D semielliptic cylinder of contrasting thermal conductivity. Using the analytical solutions (Appendix 2) from Lachenbruch and Marshall (1966), we assign a uniform heat flow from below that is equal to the Brunei mean (77.6 mW/m^2). To reproduce our observed surface heat flow with this simple model, it is necessary to invoke an order of magnitude contrast between the thermal conductivities inside and outside the trough (Figure 6). This contrast (K = 10, Appendix 2) approximates a change in thermal regime from conductive (inside the trough) to convective (outside the trough). Outside the sediment trough, faulted basement highs or fault zones provide conduits for vertical fluid flow and the seeps targeted by our survey. From model 1 (Figure 6), a trough with a half-width–to–depth ratio (hw/*d*) of 30 can be seen to produce a departure from our mean heat flow to account for our highest observed heat flow at the sediment-fault zone boundary. Model 2 (hw/*d* = 1.2) reduces heat flow in the interior of the trough to our lowest observed values.

The reliable means (Sclater et al., 1976) in Figure 3 represent data obtained from sediment ponds greater

than 200 m (660 ft) thick, believed to inhibit the influence of hydrothermal circulation on the data. Some investigators apply this strategy to surface geochemical surveys and deliberately position heat-flow sites away from geochemical sites, where heat flow is expected to be uniform and more indicative of regional means. Our model results (solid curves and lines, Figure 6) predict uniform heat flow within the trough; however, mean regional heat flow is significantly reduced (R). Accordingly, heat-flow measurements within a 200-m (660-ft)-thick sediment trough with a 12-km (7.5-mi) spacing between fault zones (hw/d = 30, model 1) would underestimate mean regional heat flow by R = 23%. For shallower troughs with narrower fault zone spacing (e.g., hw/d = 1.2, model 2), it can be seen that this underestimation can be several times greater (Figure 6). To reliably define mean regional heat flow (the inverse problem), our model results support the need for a representative data sampling of the full spectrum of heat flow. Even if subbottom geometry is known exactly, correction of interior trough measurements is impossible without the confirmation of active fluid flow and an estimate of its rate. These can only be provided by heat-flow measurements within zones of anticipated vertical fluid migration, as in the present survey. Hence, using the model of Bredehoeft and Papadopulos (1965) (Appendix 3), we calculate the rate of fluid flow from depth required to produce the maximum heat flow (604 mW/m^2) observed at the megaseep (assuming the Brunei mean regional heat flow of 77.6 mW/m^2). This yields a flow rate of 1.7 cm/yr (0.67 in./yr) from 6 km (3.6 mi) depth, the approximate maximum depth of faulting associated with the Baram delta pseudo–accretionary prism (AP, Figure 2). In our geological setting, vertical water flow represents the most likely explanation for the high megaseep heat flow. Independent of the geochemistry, heat flow this high constitutes strong evidence for characterizing the megaseep as a localized site of active fluid flow from depth.

We can also apply our simple trough model (Figure 6) to the large-scale distribution of heat flow and surface hydrocarbons in our survey area (Figures 2, 4). Accordingly, the interior of the model 1 trough (Figure 6) simulates at 59.7 mW/m^2 our Palawan Trough heat-flow data (59.0 mW/m^2). The adjacent convective zone simulates our landward data with the highest heat flow (~600 mW/m^2) produced at the contact between the two, simulating the decollement and the megaseep heat flow.

Geological Implications

For the passive Norwegian margin, Ritter et al. (2004) express the minimum degree of focusing of fluids along faults as the ratio of the flow rate to the sedimentation rate, the upper limit to compaction-driven flow (Bjørlykke, 1993). Sedimentation rates at depths similar to ours (~1500 m; ~4921 ft) reported for the nearby Sarawak Basin average 500 m/m.y. (1640 ft/m.y.) (0.05 cm/yr; 0.02 in./yr) over the last 3 m.y. (Mat-Zin and Swarbrick, 1997). This implies more than 30 times focusing of the 1.7-cm/yr (0.67-in./yr) (5.5×10^{-10}-m/s; 1.80×10^{-11}-ft/s) flow required to account for the megaseep heat flow, at least three times the values estimated by Ritter et al. (2004). Based on our heat-flow distribution (Figure 4), this flow (arrow, Figure 2) may be channeled along low-angled landward-dipping faults associated with the Baram delta pseudo–accretionary prism. Fluid expulsion along similar faults is supported by abundant data from the Barbados accretionary complex (Fisher and Hounslow, 1990; Langseth and Moore, 1990; Langseth et al., 1990; Screaton et al., 1990; Vrolijk et al., 1991) and the Costa Rican margin (Langseth and Silver, 1996; Ruppel and Kinoshita, 2000). Fluid flow predominates along decollement zones feeding the low-angle faults, where Darcy velocities from 10^{-9} to 10^{-7} m/s (3.3×10^{-9} to 3.3×10^{-7} ft/s) with maximum permeability 10^{-12} m^2 (10^{-11} ft^2) (~1000 md) have been calculated (Fisher and Hounslow, 1990; Screaton et al., 1990). Davis et al. (1990) calculate a uniform vertical flow velocity of 8×10^{-10} m/s (2.6×10^{-9} ft/s) for the northern Cascadia accretionary prism. The similarity of our Baram delta pseudo–accretionary prism data results to active accretionary complexes exists despite the passive status that our survey area now holds. Faults in subsiding basins are not likely to be open because they are generally less permeable than the surrounding ductile sediments (Bjørlykke, 1999; Fisher et al., 2003). Higher temperatures could be the overriding factor. Higher heat flow observed for the landward sediments of the Baram delta and, correspondingly, higher temperatures at shallower depths facilitate flow (Fisher et al., 2003) in the absence of the forces of active subduction. A history of episodic rifting (Ru and Pigott, 1986) may also exert alternating degrees of extensional and compressional influence on our study area. This would help to keep faults active and to propel fluids.

In addition to the driving pressure, the sources of fluids under active margin tectonics (e.g., Vrolijk et al., 1991) may not be available in our area. To duplicate

maximum flow in the Barbados accretionary prism requires pressures of up to 2.5×10^6 Pa (Fisher and Hounslow, 1990), which can be developed in only 250 m (820 ft) differential hydraulic head. Reservoir rock permeability up to 1900 md has been reported for the Brunei–Sabah margin (Blanche and Blanche, 1997), exceeding that calculated for Barbados (Fisher and Hounslow, 1990). Hence, in our study area, tropical highlands along the coast of Borneo, culminating in 4101 m (13,455 ft) Mt. Kinabalu, are more than capable of supplying water under sufficient pressure to any part of the adjacent margin. Water (Figure 2, arrow) may descend along terrestrial faults to the decollement zone at about 6 km (3.6 mi) depth below seabed. It may then ascend to the seabed via landward-dipping faults to produce the observed heat flow and hydrocarbon distribution (Figure 4). This flow can also be seasonal and transient under Darcian flow conditions (Fisher and Hounslow, 1990).

Time Constraints

The relationship between heat and fluid flow and the presence of thermogenic hydrocarbons in the sediments implies that certain time constraints are met. The vertical fluid flow needed to produce the megaseep heat-flow anomaly (1.7 cm/yr; 0.67 in./yr), requires 3.5×10^5 yr for fluids to reach the seabed from 6 km (19,700 ft) depth. Well data from various parts of the region indicate sufficient maturity for significant hydrocarbon generation from 2133 to more than 3353 m (7000 to 11,000 ft) (Blanche and Blanche, 1997). Hence, it requires about 1.8×10^5 yr for hydrocarbons generated at 3000 m (9840 ft) depth to reach the seabed if carried along with the water flow from depth. This time is about 1% of the middle Miocene (~14 Ma) to late Oligocene (~25 Ma) ages of important source rocks for the Brunei–Sabah basin (Blanche and Blanche, 1997). If source rocks at 3000 m (9480 ft) average 20 m.y. in age, the average subsidence rate (150 m/m.y.; 492 ft/m.y.) implies 27 m (89 ft) of subsidence (~1% of depth) in the time it takes fluids to reach the seabed and to supply proposed reservoirs, thought to be no younger than the late Miocene (~10 Ma) (Blanche and Blanche, 1997).

Zielinski and Bruchhausen (1983) showed that water flow could account for both long-range hydrocarbon migration and high heat flow in the Magellan Basin (Argentina). The same appears true for the Brunei margin, provided that significant hydrocarbon generation has predated about 2 Ma. This does not preclude more rapid migration by bubble ascent or continuous gas-phase flow in fractures (Brown, 2000). We compare the relative effects of water-borne and gas-phase migration for the same model (Bredehoeft and Papadopulos, 1965) already applied to the megaseep in Appendix 3. Offsetting the reduced heat transport capacity of gas compared to water, under the exact same conditions, the model predicts that an upward gas velocity $v_{zg} = -2.3 \times 10^{-8}$ m/s (-7.5×10^{-8} ft/s) (-72.5 cm/yr; -28.5 in./yr) can also account for the megaseep heat-flow anomaly. This is 42 times greater than that for water; however, even higher gas-migration velocities are possible (Brown, 2000).

MEGASEEP DATA RESULTS

From the procedure outlined in Appendix 4, Figures 7–14 reveal in the megaseep data (dashed lines) direct and inverse correlations between heat flow and geochemical parameters representing the spectrum of analyses performed. We observe three basic categories of correlation. In the first, hydrocarbon concentrations and heat flow at the megaseep (dashed lines) increase proportionally to significantly exceed all or most values for the remaining regional survey data. This category includes virtually all of the hydrocarbon data as exemplified by adsorbed gases (Figure 7) and the extracted organic matter (EOM) data (Figure 8). The geochemical data provide strong evidence for active vertical fluid migration and seepage of thermogenic hydrocarbons from depth at the megaseep. Furthermore, in the absence of a shallow igneous body or salt dome, vertical fluid flow (Bredehoeft and Papadopulos, 1965) is the only reasonable mechanism to account for the observed high heat flow, in excess of 500 mW/m^2.

For the second correlation category, systematic changes in megaseep heat flow and hydrocarbons represented by EOM data (Figure 9), biomarker abundances and ratios (Figures 10–12), and isotope data (Figures 11, 12) are evident (dashed lines). However, unlike category 1 data, category 2 megaseep and regional (solid lines) hydrocarbon data ranges are comparable, suggesting common origin. This is remarkable considering that the megaseep data (dashed lines) represent a distance of less than 500 m (1600 ft) (Figure 15); whereas the regional data span distances on the order of 100 km (60 mi). Data patterns apparent in two aromatic sterane ratios are mirrored in isotope data in Figures 11 and 12, also reflecting common genesis.

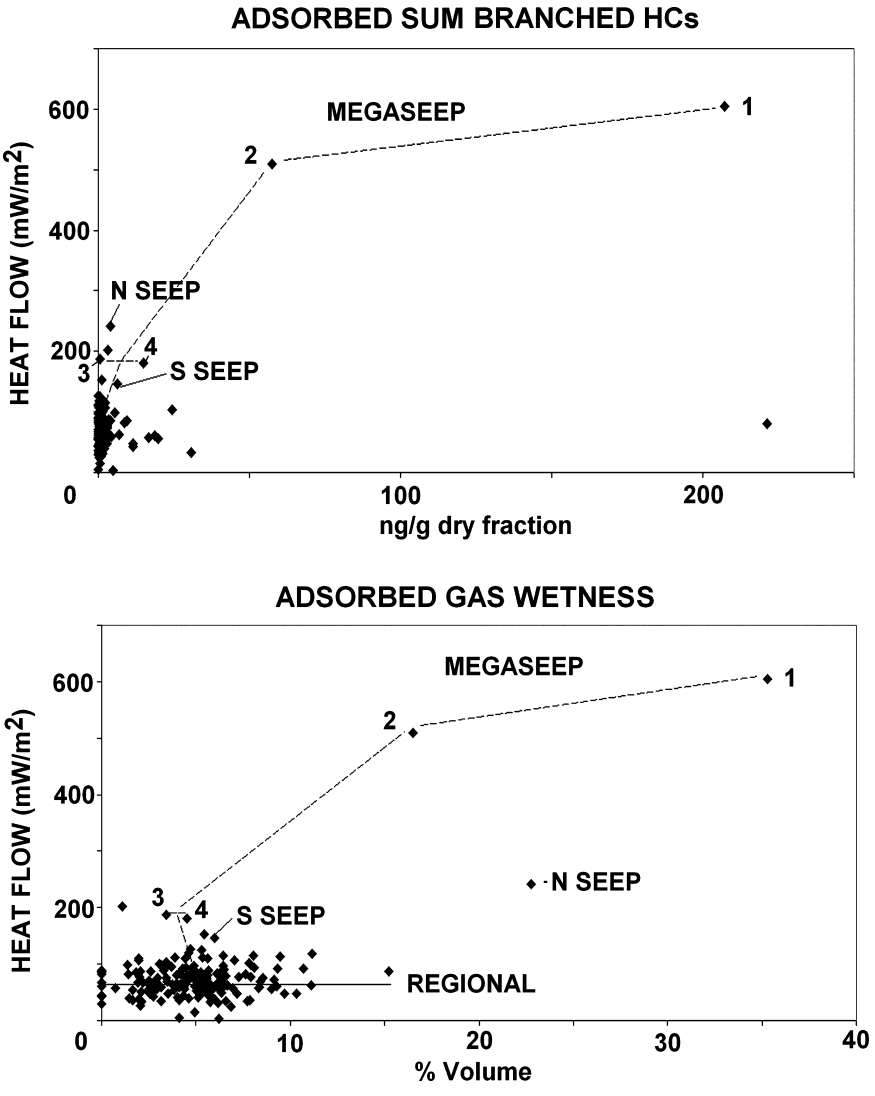

Figure 7. Crossplots of heat flow versus two adsorbed category 1 hydrocarbon parameters, where megaseep values (dashed lines) far exceed the remaining regional or background data (solid line). Wetness = $(C_2 + C_3 + C_4)/(C_1 + C_2 + C_3 + C_4)$, N and S seeps are 10 and 15 km (6 and 9 mi), north and south, of the megaseep.

For the third category of correlation, hydrocarbon parameters appear relatively invariant at the four highest heat-flow megaseep sites (sites 1–4, Figure 15), but convert to background levels by the outlying sites 5–7, where data are available. The represented hydrocarbon ratios (Figures 13, 14) constitute the largest wavelength anomalies associated with the megaseep, extending the greatest distances from the seep axis (Figure 15). They also appear to span a large fraction of the regional data range, where outlying site (5–7) data are available (e.g., upper plots, Figures 13, 14). This is similarly reflected in the EOM data (Figure 9), where values also remain relatively high for the four primary megaseep data points (right side) and decrease significantly thereafter (left) to background values.

The correlation, trend, and wavelengths of megaseep geochemical data and heat flow are shown in Figure 16, a plot of concentration (or parameter value) relative to the concentration or value observed at site 1 for the seven megaseep sites located in Figure 15. Figure 16 includes most of the examples in Figures 7–14. For the Figure 11 monoaromatic sterane ratio (marst) and the Figure 13 ratio of alkenes to n-alkanes (1-adC_{2-6}alkenes/nalk), one minus the values ($1 - v$), then normalized to site 1, are plotted in Figure 16. One minus values are used for plotting purposes because these parameters, in contrast to the others, increase with increasing site number and distance from the seep axis. The dashed lines indicate missing data, where no $\delta^{13}C$ isotopic data, e.g., adsorbed propane ($ad^{13}C_3$) were obtained for site 3. The anomalous adsorbed methane value (adC_1) for site 4, at seven times the value at site 1, is probably biogenic and is omitted. No biomarker or isotope data were obtained for sites 5–7 because those sites did not meet minimum screening criteria to warrant those analyses. The biomarker and

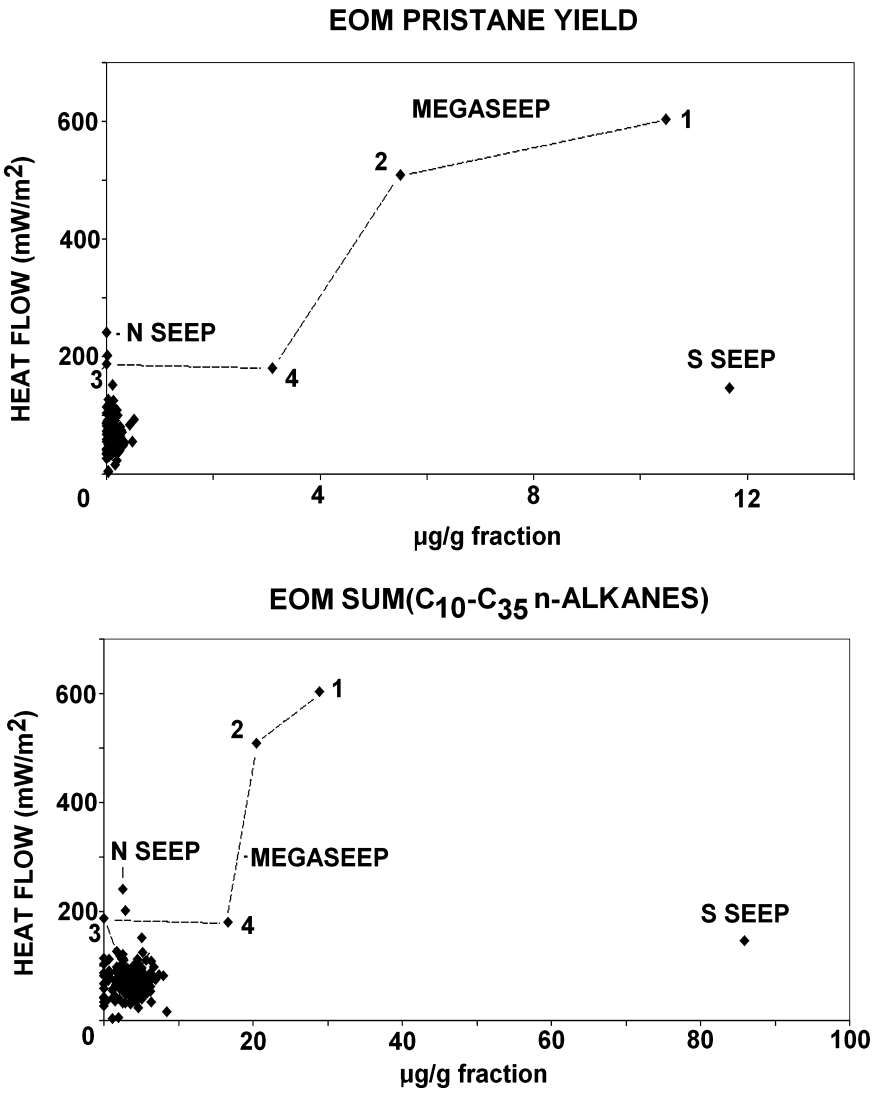

Figure 8. Crossplots of heat flow versus two EOM (bitumen) category 1 hydrocarbon parameters, where megaseep values (dashed lines) far exceed remaining regional or background data, except for the S seep. N and S seeps are 10 and 15 km (6 and 9 mi), north and south, of the megaseep.

isotope values for sites 5–7 in Figure 16 are extrapolated from their respective crossplots (Figures 10, 11) and are assumed constant at all three sites. These extrapolations appear reasonable in light of the reason for limited analyses for the sites. The general decline in heat flow (large solid squares) appears centrally located amidst the corresponding geochemical data in Figure 16.

Megaseep Models

Based on the megaseep data and their relative positions (Figure 15), we have constructed two simple models for evaluating the Figure 16 data results. First (Figure 17), we find excellent agreement between observed megaseep heat flow and that produced by a simple buried line source model (Von Herzen and Uyeda, 1963) for a seep oriented nearly east-west at site 1 (dashed line, Figure 15). This happens to be subparallel to the South China Sea Basin magnetic lineations (Taylor and Hayes, 1983). In Figure 17, the megaseep heat-flow data (solid squares) are plotted versus the distance from the inferred megaseep axis, and the solid curve is the theoretical model result for an infinite line source buried 157 m (515 ft) below the sea floor (Appendix 5). The higher-than-theoretical values observed at sites 6 and 7 reflect the decay of anomalous megaseep heat flow below background heat flow (not included in our model) beyond 400 m (1312 ft) from the inferred seep axis. By substituting concentration for temperature (Appendix 5), the same model can be used to assess the function of broadly defined mass diffusion on the megaseep geochemical data. Because of the constant surface boundary condition at the sea floor, we computed relative concentration (C/C_o) values for both

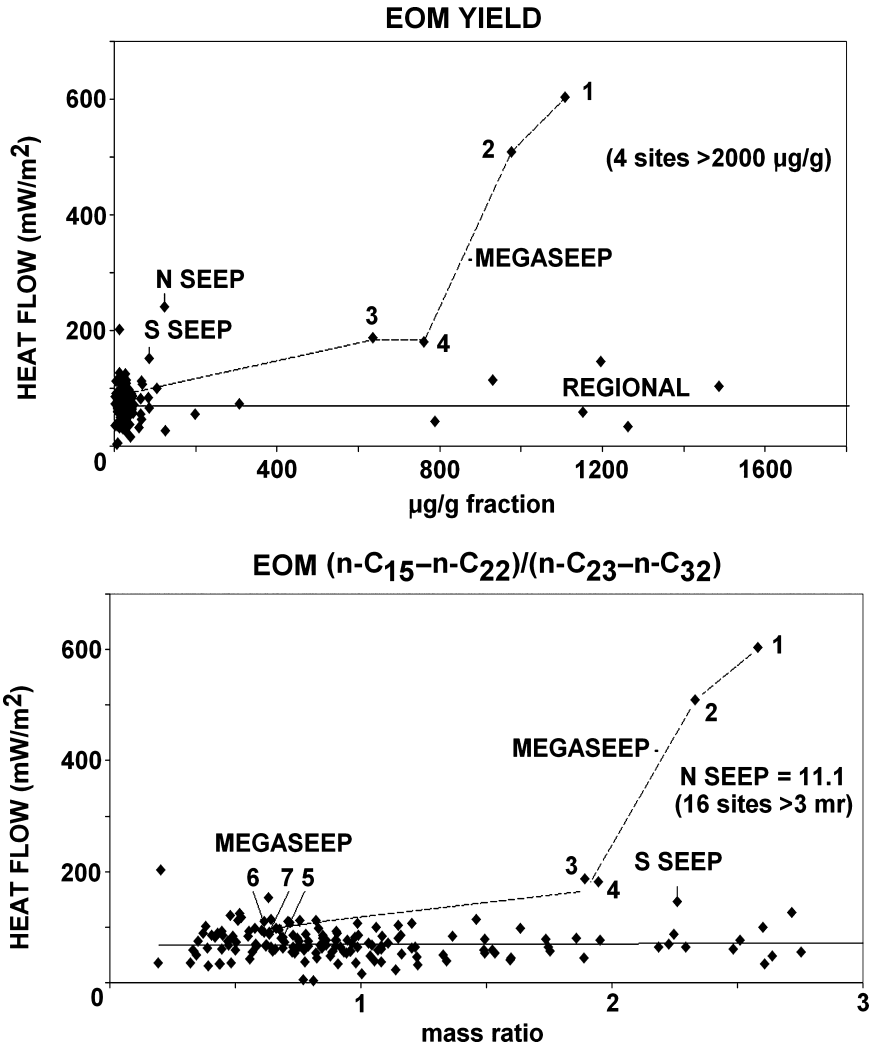

Figure 9. Crossplots of heat flow versus two EOM (bitumen) category 2 hydrocarbon parameters, where high-heat-flow megaseep data branches (dashed lines) have data ranges comparable to regional (solid lines). The lateral scale of the megaseep data is about 700 m (2296 ft), and the lateral scale of the regional data is approximately 100 km (60 mi). See Figure 15 for megaseep, north (N), and south (S) seep relative locations. mr = mass ratio.

1 and 4 m (3.3 and 13 ft) below the surface, observing no significant difference between the two.

In the second model (Appendix 6), we test the possibility that the correlation of heat flow and geochemistry at the megaseep (Figure 16) results directly from increased thermogenesis caused by higher heat flow. Increased thermogenesis can result from exposure of organic material to higher temperatures because of higher heat flow over its geohistory. Localized examples may include salt domes (Rashid and McAlary, 1977) and hydrothermal petroleum (Simoneit and Lonsdale, 1982). For a first approximation and for mathematical simplicity, we follow Waples (1980), assuming that organic material beneath megaseep site 4 is at the onset of thermogenesis. We then calculate the increases in concentrations (C/C_o) from increased thermogenesis caused by the higher heat flow observed at each successive site (3 to 1). We first do this for a geotherm produced by simple steady vertical heat conduction. Then, we assume that vertical fluid flow (the only geologically plausible mechanism) creates the megaseep heat-flow anomaly. The latter geotherm is calculated according to Bredehoeft and Papadopulos (1965). Details are in Appendix 6.

Megaseep Model Results

The diffusion model results for source depths of 157 m (515 ft) (diffusion 157), the same used to model heat flow (Figure 17), 34 m (111 ft) (diffusion 34), and the thermogenic model results computed for conductive (COND) and convective (CONV) geotherms are plotted in Figure 18. Selected data from Figure 16 are also plotted in Figure 18. Despite being roughly equidistant from the seep axis, some geochemical data differences between sites 3 and 4 are apparent. This is also seen in the crossplots (Figures 7 –14). Because there are two separate migration paths from the axis

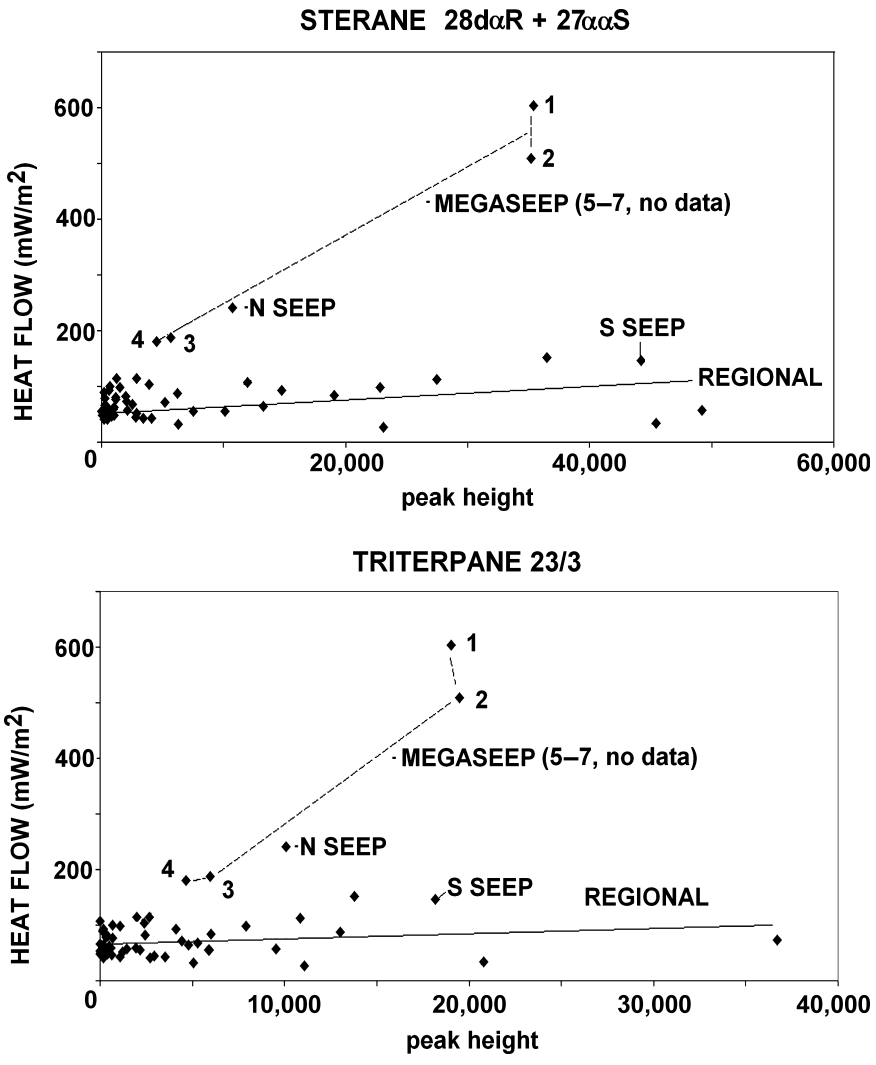

Figure 10. Crossplots of heat flow versus two biomarker peak heights, category 2 hydrocarbon parameters, where high-heat-flow megaseep data branches (dashed lines) have data ranges comparable to regional (solid lines). The lateral scale of the megaseep data is approximately 250 m (820 ft), and the lateral scale of the regional data is about 100 km (60 mi). No data exist for megaseep sites 5–7; however, plots extrapolate to regional and background values (≈0). See Figure 15 for megaseep, north (N), and south (S) seep relative locations. 28d = C_{28} diahopane; 23/3 = C_{23} tricyclic.

to these sites (Figure 15), some real-data differences are not surprising.

Megaseep data generally reflect patterns exhibited by the diffusion model for source depths of 34 and 157 m (111 and 515 ft). Headspace gas data represented by propane (hsC_3) can be accounted for by even shallower source depths. More invariant (category 3) parameters represented by the ratio of alkenes to n-alkanes (1-adC_{2-6}alkenes/nalk) can be simulated by a broader source distribution as demonstrated by Von Herzen and Uyeda (1963) and deeper source depths (<1 km; <0.6 mi). However, the thermogenic model (COND and CONV) appears capable of accounting for only hydrocarbon gas data, represented in Figure 18 by headspace propane (hsC_3) and by adsorbed and occluded sums of branched hydrocarbons (adsumbranched and ocsumbranched). Some of the departure among and between parameters and the thermogenic model results (Figure 18) could reflect real differences in kinetic constants not accounted for by Waples (1980) and in Appendix 1.

In Figure 13, the triterpane ratio $T_s/(T_s + T_m)$, which can indicate both thermal maturity and source (Moldowan et al., 1986), appears decidedly invariant at megaseep sites 1–4, where heat flow varies most significantly. This invariance holds true for 20S/(20S + 20R) C_{29} sterane (C_{29}ααα20S), C_{29}ββ/(ββ + αα) sterane, 30d/(30d + 29βα) terpane ratios, and the aromatic MPI (Radke et al., 1982; Radke and Welte, 1983; Radke, 1987), all potential thermal-maturity indicators (e.g., Peters et al., 2005). Plotted relative to heat flow (Figure 19), they show little variation compared to heat flow and no consistent sitewise variation. In contrast, the Figure 11 monoaromatic sterane C_{21}M/(C_{21}M + βSC_{28}MA) (marst) appears to mirror relative heat flow in Figure 19. However, it increases with decreasing heat flow, the opposite of the trend expected if heat flow were causally linked to thermal

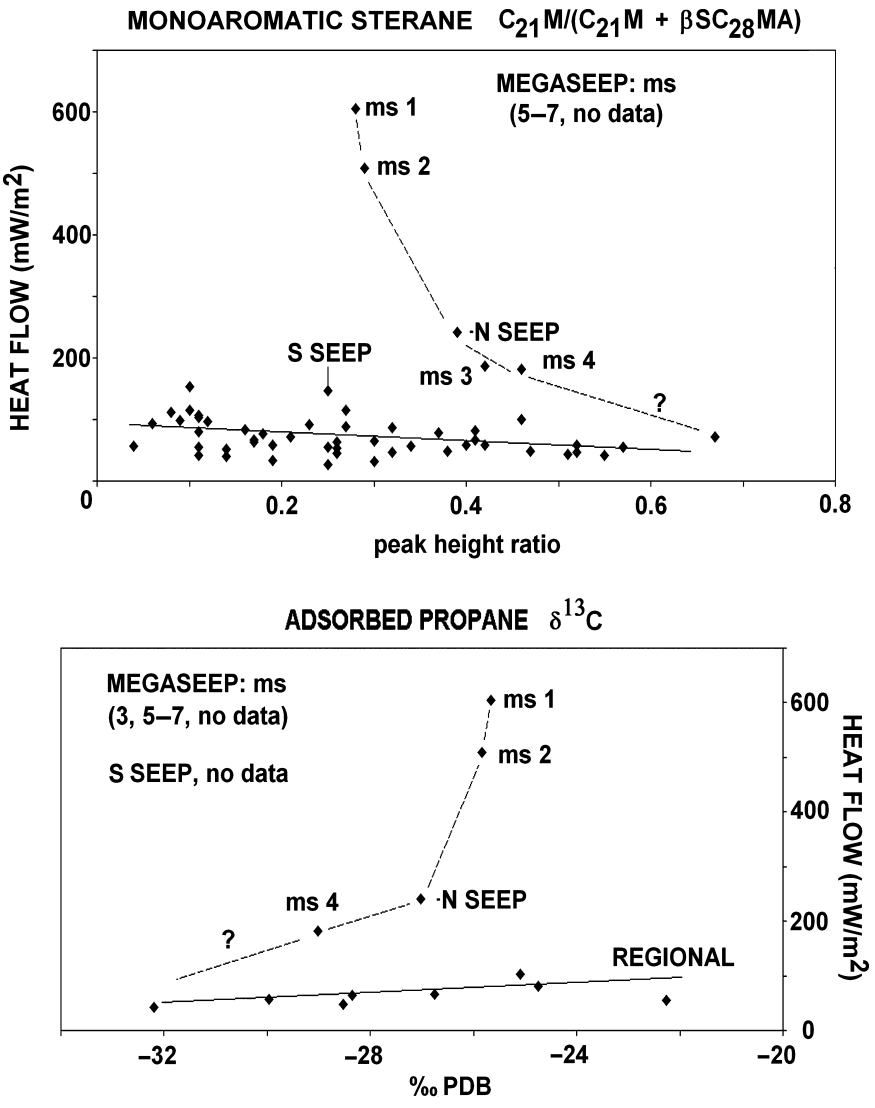

Figure 11. Crossplots of heat flow versus two category 2 hydrocarbon parameters, where high-heat-flow megaseep and north (N) seep data branches (dashed lines) have data ranges comparable to regional (solid lines). The lateral scale of the megaseep data is about 250 m (820 ft), and the lateral scale of the regional data is approximately 100 km (60 mi). The biomarker ratio (monoaromatic sterane in Figures 16 and 19) and isotope data (lower, no S seep value) exhibit the same pattern, reflecting common genesis. No data exist for megaseep sites 5–7; however, plots extrapolate to regional and background values. See Figure 15 for megaseep, north (N), and south (S) seep relative locations. PDB = Peedee belemnite standard.

maturity (e.g., Peters et al., 2005). The total scanning fluorescence (TSF) ratio R1 (Brooks et al., 1983, 1986) also mirrors heat flow and is the only potential maturity parameter with values at megaseep sites 5–7, where it increases to a maximum of 3.4 (C/C_o) at site 7 relative to site 1. This could indicate correlation with heat flow and thermal maturation; however, Barwise and Hay (1996) also associate increasing R1 with increased biodegradation. Based on the other potential maturation parameters (Figures 13, 19), we conclude that biodegradation is reflected in the R1 data. Sterane biodegradation is highly variable depending on conditions (Peters et al., 2005). However, a combination of processes, including near-surface biodegradation, fractionation during transport and migration, and mixing with recent organic material (ROM), instead of thermal maturation, similarly explains the change of the monoaromatic sterane ratio (marst, Figure 19). Overall, data and model results support a near-surface origin (<1 km; <0.6 mi) for the correlation between geochemistry and heat flow at the megaseep (Figures 16, 18), with processes represented spatially and temporally by concomitant molecular and thermal diffusion.

Discussion

Results indicate a lack of causal connection between correlated heat flow and hydrocarbon geochemistry at the megaseep and the predominance of the diffusion model over the thermogenic model to explain the correlation. The data and diffusion model trends (Figures 16, 18) represent transport, near-surface alteration, biodegradation, fractionation, and mixing with ROM (e.g., Mason and Evans, 1969; Mason and Marrero, 1970; Bernard et al., 1977; Brooks et al., 1979; Abrams,

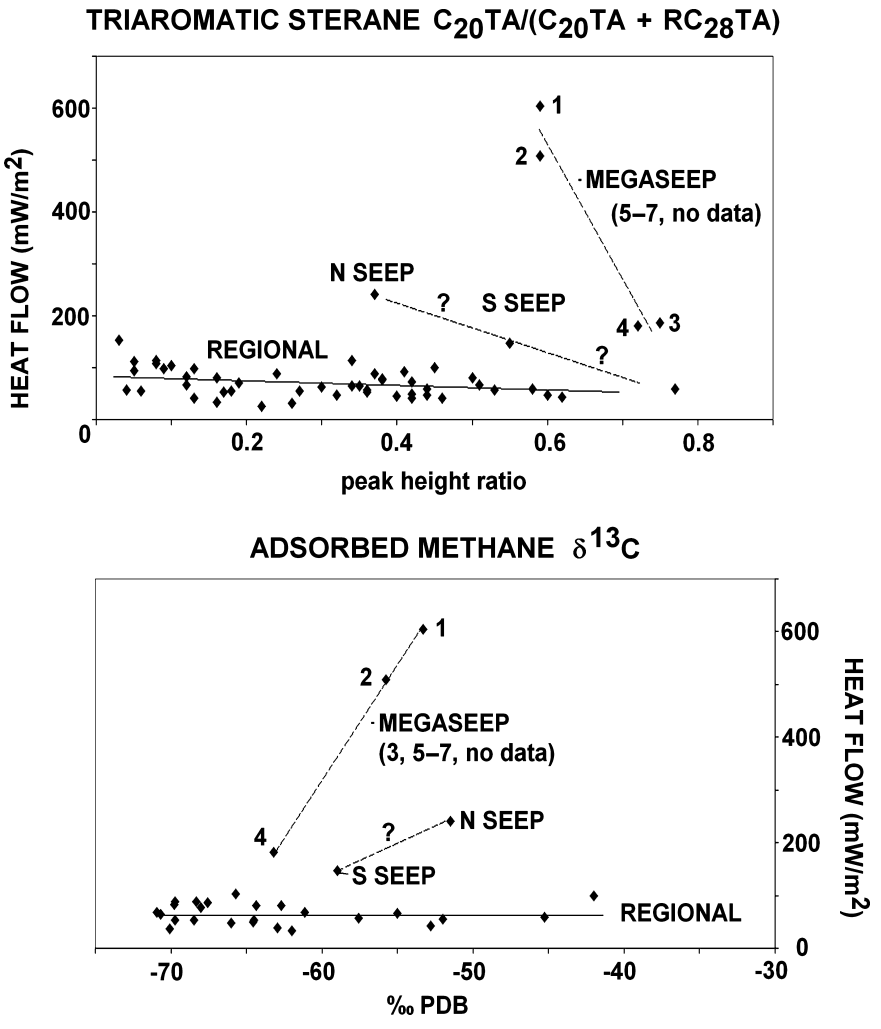

Figure 12. Crossplots of heat flow versus two category 2 hydrocarbon parameters, where high-heat-flow megaseep and north (N) seep data branches (dashed lines) have data ranges comparable to regional (solid lines). The lateral scale of the megaseep data is about 250 m (820 ft), and the lateral scale of the regional data is approximately 100 km (60 mi). The biomarker ratio and isotope data exhibit the same pattern, reflecting common genesis. No data exist for megaseep sites 5–7; however, plots extrapolate to regional and background values. See Figure 15 for megaseep, north (N), and south (S) seep relative locations. PDB = Peedee belemnite standard.

1996a, b; Sassen et al., 2003, 2004). Decreases in $\delta^{13}C$ and hydrocarbon gas wetness = $(C_2 + C_3 + C_4)/(C_1 + C_2 + C_3 + C_4)$ with distance from the megaseep axis support this conclusion. Figure 16 provides a unique record of the evolution of multiple hydrocarbon parameters that are relatively fresh at site 1 (caused by more active seepage) toward their respective background values (sites 5–7). Understanding these transformations is important for correlating sea-floor hydrocarbons with their possible sources at depth (e.g., Peters et al., 2005). The availability and use of multiple independent and interrelated parameters help discriminate between the basic models in this study (Figures 18, 19). Patterns corroborated by multiple parameters (e.g., Figures 11, 12) should likewise lead to improved models of hydrocarbon seeps.

For category 2 parameters (Figures 9–12), the simplest explanation for comparable ranges of megaseep (dashed lines) and regional (solid lines) data is that the latter represent former megaseeps, where high heat flow has largely decayed but the geochemical fingerprints remain relatively unchanged. A large ratio of thermal to chemical (molecular) diffusion facilitates this, and thermal diffusion coefficients are commonly cited at several orders of magnitude greater than molecular diffusion coefficients (e.g., Von Herzen and Uyeda, 1963; Mason and Marrero, 1970). Hence, the category 2 regional data appear in crossplots as the cumulative result of site-specific sampling (Abrams, 1996a) at random distances (<500 m; <1640 ft) from geochemical megaseeps. These data largely reflect the same near-surface (<1-km; <0.6-mi) processes seen at the megaseep instead of true regional variations. Under this hypothesis, individual samples from 100 seeps appear indistinguishable from 100 samples from a single seep. A potentially useful consequence is that distances from seeps and paleoheat flow for each regional seep site can be inferred from the megaseep data. This is exemplified for one regional site (X) and one parameter ($\delta^{13}C_3$) in Figure 20.

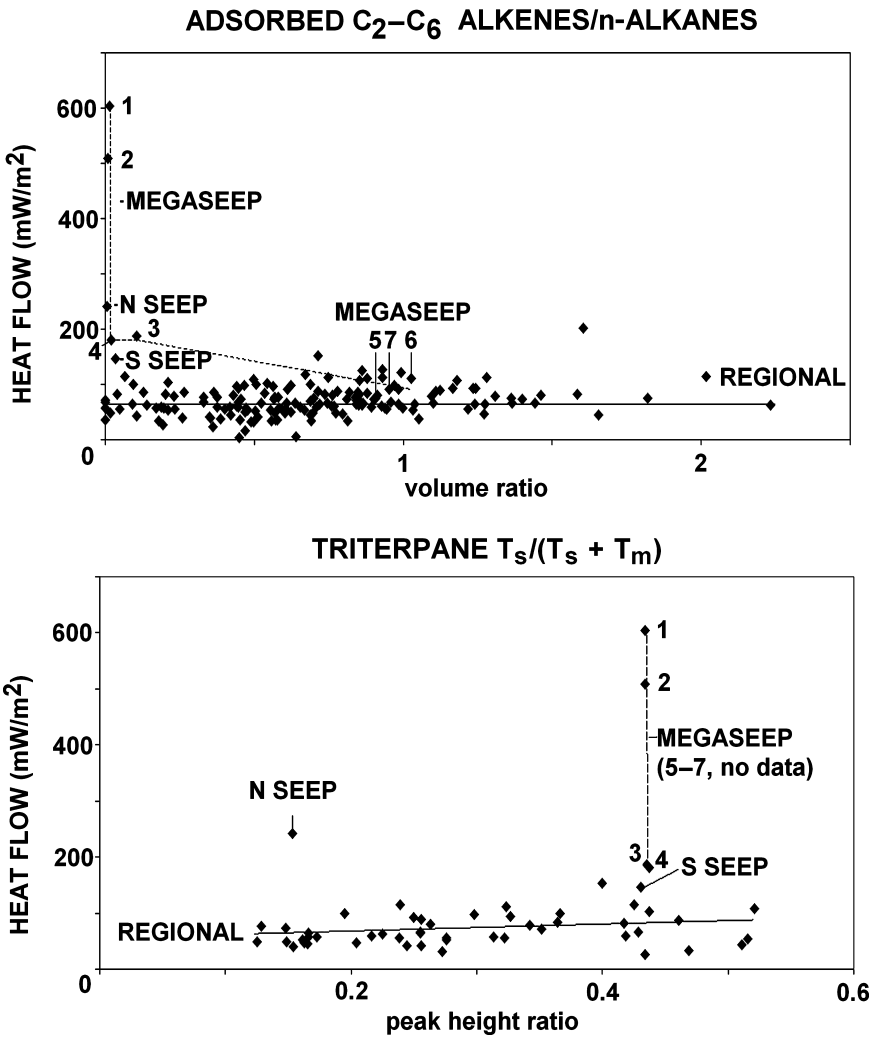

Figure 13. Crossplots of heat flow versus adsorbed and biomarker ratios, category 3 hydrocarbon parameters, which are comparatively invariant in the primary (sites 1–4) megaseep data (dashed lines), i.e., across the 250-m (820-ft) half-width of the megaseep. Outer megaseep sites 5–7 reflect a rapid fall to background levels. No site 5–7 biomarker data exist. See Figure 15 for megaseep, north (N), and south (S) seep relative locations. Solid lines indicate regional data branches. T_s and T_m are C_{27} hopanes, 18α-22,29,30-trisnorneohopane and 17α-22,29,30-trisnorhopane.

Regional data in several category 2 crossplots (Figures 9–12) are shown with trends (solid lines) that correspond in slope with megaseep data trends (dashed lines). The regional trends are somewhat speculative because the heat-flow data appear scattered about the regional lines, and correlation coefficients for regional data regressions are low. Scatter in the regional heat-flow data most likely reflects regional seeps in differing stages of thermal decline and, correspondingly, more or less active in terms of flow rates. Hypothetical regional data points plotting vertically just above and just below site *X* in Figure 20, for example, would indicate the same distance from seeps that are, respectively, more and less active than seep *X*. The single regional data point significantly outside the megaseep data range ($\delta^{13}C_4 > -24‰$) would indicate a paleoheat flow greater than 604 mW/m^2.

Statistics commonly applied to drilling programs (e.g., Davis, 1986) support the paucity of undiscovered megaseeps within our survey area as follows. Of the four primary megaseep sites (sites 1–4, Figure 15), two resulted in decidedly anomalous heat flow and geochemistry (i.e., 50% success). If we argue that four sites were required to discover the megaseep, this represents 25% success. However, the two most anomalous megaseep sites 1 and 2 are unique in 186 sites for an overall success of only 1.1%. Given the discovery of the megaseep by any of four sites, the probability that no other megaseeps are observed among our regional sites is practically nil. This further supports that our regional data largely represent thermally decayed, less active megaseeps with both lower heat flow and an absence of anomalous category 1 parameters.

The ratios of some triterpanes and alkenes and n-alkanes (Figures 13, 14) and bitumen (EOM) data (Figure 9) appear less affected by megaseep processes. They remain decidedly anomalous at least 250 m (800 ft) from the megaseep axis, encompassing all

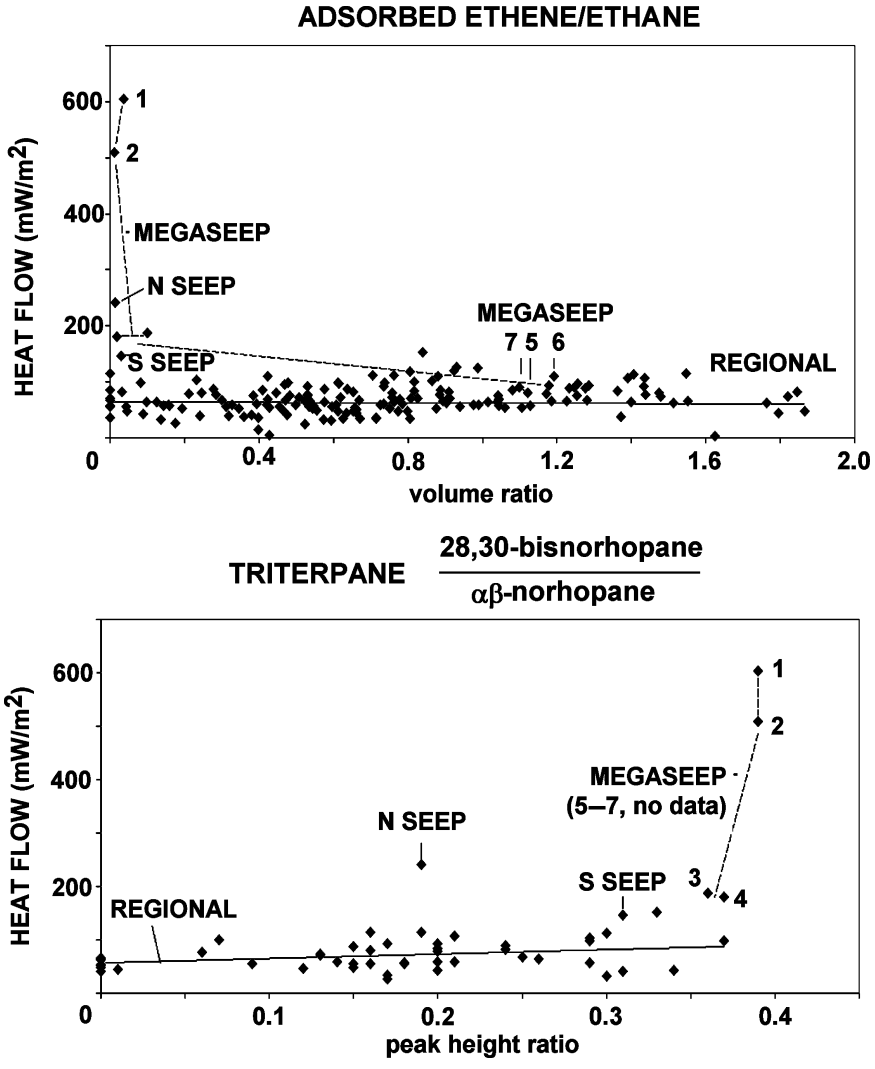

Figure 14. Crossplots of heat flow versus adsorbed and biomarker ratios, category 3 hydrocarbon parameters, which are comparatively invariant in the primary (sites 1–4) megaseep data (dashed lines), i.e., across the 250-m (820-ft) half-width of the megaseep. Outer megaseep sites 5–7 reflect a rapid fall to background levels. No site 5–7 biomarker data exist. The terpane ratio is singularly maximum at the megaseep. See Figure 15 for megaseep, north (N), and south (S) seep relative locations. Solid lines indicate regional data branches.

four high heat-flow sites (Figures 16, 18). Like casting a significantly larger net, this invariance in category 3 parameters constitutes a significantly greater aperture for detecting seeps in surface geochemical data. This can be compared with headspace gases (e.g., hsC_3), observed anomalous only at site 1. Like heat flow, category 1 adsorbed gases, and EOM parameters (Figures 7, 8), 28,30-bisnorhopane/αβ-norhopane (Figure 14) and alkenes/n-alkanes (Figures 13, 14) exhibit megaseep values that are extreme compared with most other sites. The Figure 11 monoaromatic sterane (marst) $C_{21}M/(C_{21}M + \beta SC_{28}MA)$ additionally shows sitewise correlation with heat flow (Figure 19). Like heat flow, these parameters may, in combination, define more active seepage, where migration to the surface is more rapid and more recent, and hydrocarbons are least altered by effects of biodegradation (e.g., Tissot and Welte, 1978; Hunt, 1979; Waples, 1981; Peters et al., 2005). Heat-flow data results, however, are unique in being easily available while in the field.

Despite its high (604 mW/m^2) heat flow, among the highest ever reported, the adsorbed methane concentrations observed (~100 ppb) at the megaseep fall short of the approximately 1000-ppb levels required by Abrams (1996b) to be classified as active (type A), resulting in the presence of bubbles in the water column and associated benthic communities. However, based on the megaseep site distribution (Figure 15), we cannot rule out the existence of higher heat flow and higher methane concentrations just to the south. In fact, we have measured heat flow at more than twice that of the megaseep elsewhere on the northern Borneo margin. Our data results, however, support the use of heat flow to detect significant active seepage at subtype A levels. Like the megaseep, many cold seeps (e.g.,

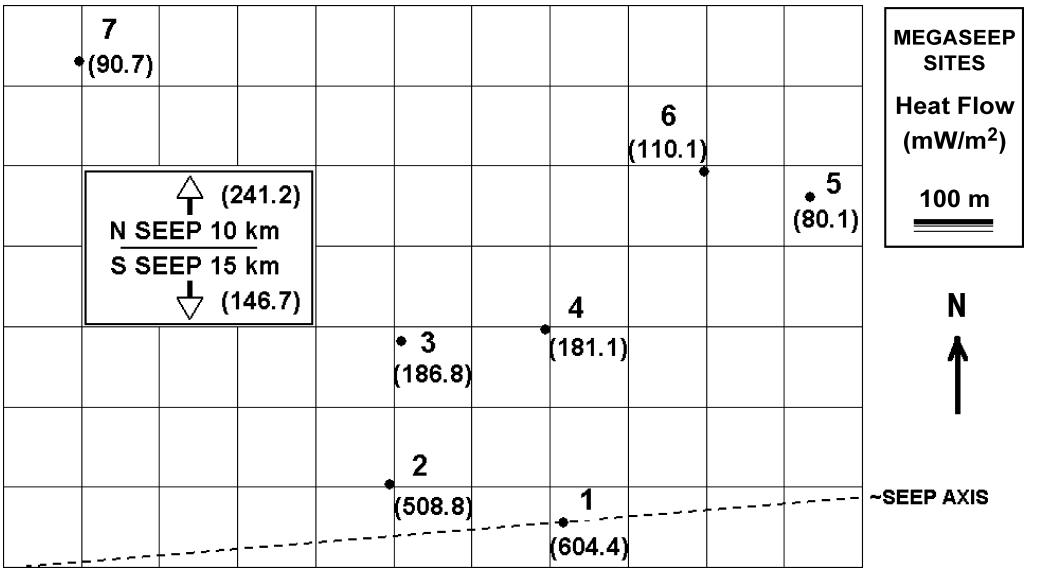

Figure 15. Relative location of the seven megaseep sites with heat-flow values (mW/m^2) in parentheses. The orientation of the inferred seep axis (dashed line) is based on the heat-flow measurements, assuming intersection with maximum heat flow site 1. Relative positions of the north (N) and south (S) seeps and heat-flow values are indicated.

Klaucke et al., 2005) may not appear cold in terms of heat flow. More data at cold seeps are needed to confirm results presented here and to assess the significance of hydrocarbon seepage at rates below those that produce heat-flow anomalies.

SUMMARY AND CONCLUSIONS

Bias in our heat-flow data caused by site-specific sampling appears negligible based on the following: (1) the equality of the Brunei mean heat flow and the

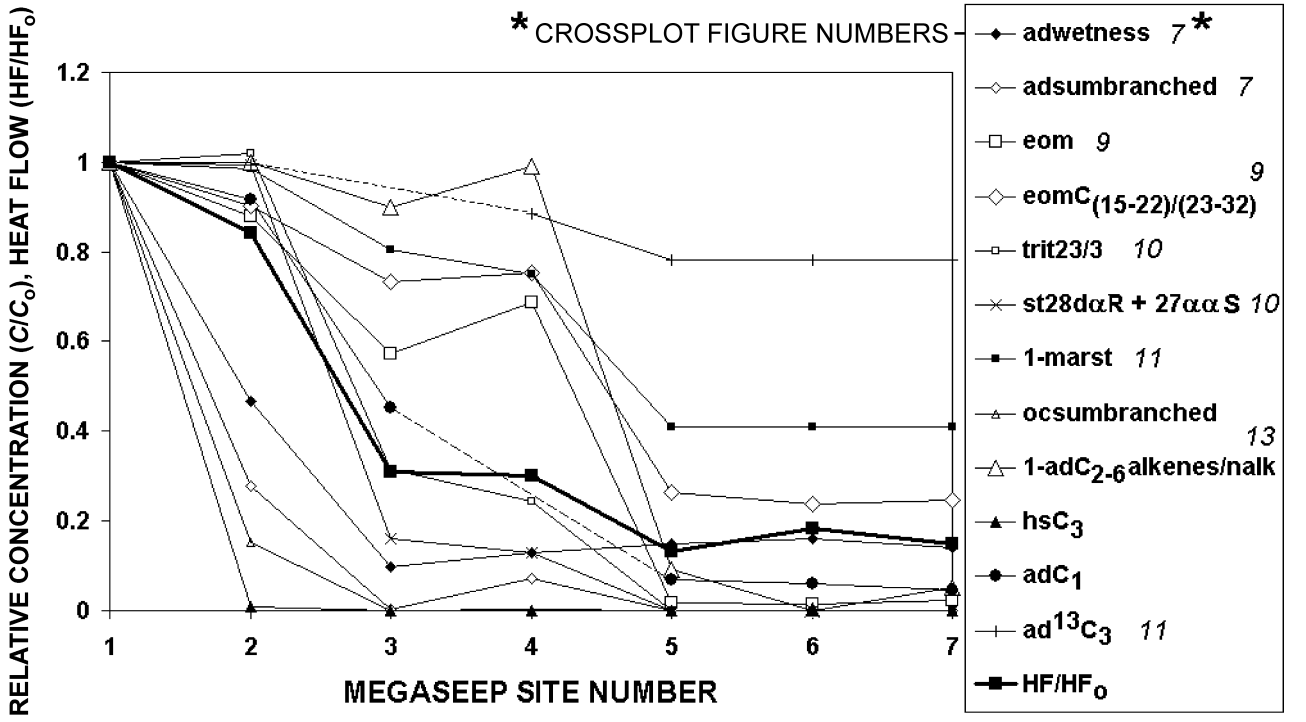

Figure 16. Megaseep observed relative concentrations (C/C_o) and relative heat flow (HF/HF_o) normalized to site 1 ($C = C_o$; $HF = HF_o$) plotted versus site number (Figure 15). Legend numbers in italics (*) indicate corresponding crossplot figure number. ad = adsorbed; eom = solvent extracted organic material/bitumen; trit = triterpane; st = sterane; marst = monoaromatic sterane; oc = occluded; hs = headspace. Dashed lines indicate missing data. Sites 5–7 biomarker (trit, st, and marst) and isotope ($ad^{13}C_3$) values are extrapolated from crossplots (Figures 10 and 11).

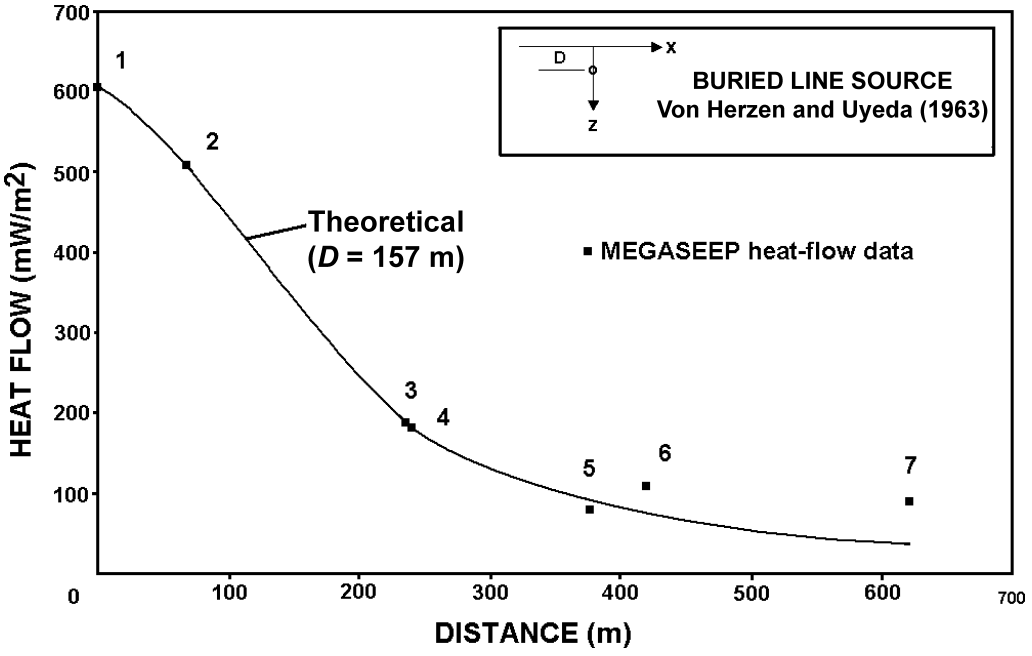

Figure 17. Megaseep heat flow (solid squares) versus distance from inferred seep axis (Figure 15). The solid curve is the theoretical heat flow versus distance from an infinite line source at depth D = 157 m (515 ft) (Appendix 5) underlying the seep axis at site 1. Theoretical heat flow falls below background data values greater than 400 m (1312 ft) from seep axis.

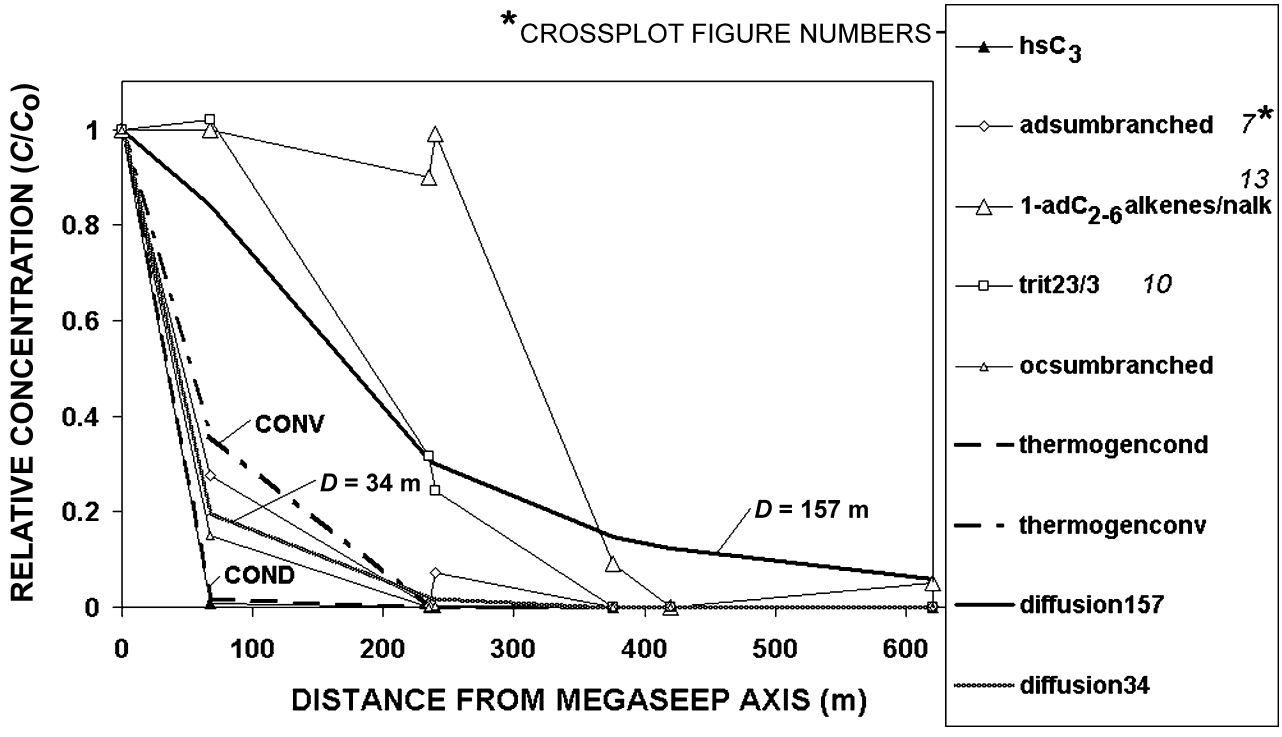

Figure 18. Selected (from Figure 16) megaseep observed relative concentrations (C/C_o, symbols) normalized to site 1 ($C = C_o$) versus distance from inferred seep axis (Figure 15). Legend numbers in italics (*) indicate corresponding crossplot figure number. The solid lines indicate the theoretical relative concentration (Appendix 5) versus distance from an infinite line source at depths D = 157 m (515 ft) (same as for heat flow in Figure 17) and D = 34 m (111 ft) (diffusion 157 and 34) underlying the seep axis at site 1. Broken lines indicate thermogenic model (Appendix 6) values. Thermogen = thermogenic; cond = conductive geotherm, conv = convective geotherm, which account for only category 1 gas data; headspace propane (hsC_3), occluded (oc), and adsorbed (ad) sum of branched hydrocarbons (sumbranched). Triterpane (trit) values greater than 300 m (984 ft) from axis ($C/C_o = 0$) are extrapolated from Figure 10. Invariant (<300 m; <984 ft) category 3 parameters, e.g., adsorbed C_{2-6}alkenes/n-alkanes (large open triangles) have longest wavelengths, and headspace gases (e.g., hsC_3, solid triangles) have the shortest.

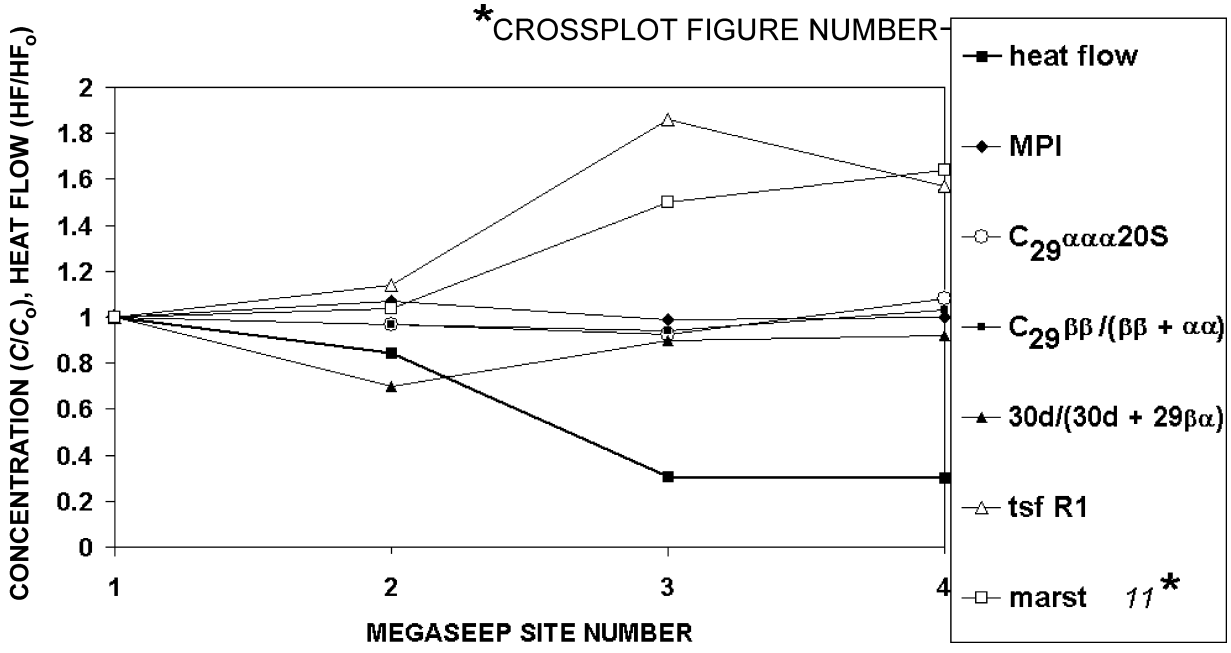

Figure 19. Relative (to site 1) heat flow (HF/HF_o) and relative concentrations ($C/C_o = 0$) of potential thermal maturation indicators, biomarkers (e.g., Peters et al., 2005), and MPI (Radke et al., 1982; Radke and Welte, 1983; Radke 1987) for megaseep sites 1–4 show no correlation. Correlation of heat flow (solid squares), the Figure 11 monoaromatic sterane (marst, open squares), and total scanning fluorescence (tsf) R1 (Brooks et al., 1983, 1986) are not related to thermal maturation (see text). The abbreviations 30d and 29βα are C_{30} diahopane and C_{29}βα-hopane.

non–site-specific China margin heat flow, implying contemporaneous age; (2) the correlation of that age with dated magnetic lineations and inferred onset of rifting and sea-floor spreading; and (3) the correlation of our data with published non–site-specific heat-flow data from the northern Borneo margin. Furthermore, model results applied to our study area demand sampling in fault zones for reliable means, whereas the elusively short wavelengths of seep anomalies limit oversampling. Heat flow and surface hydrocarbon geochemistry in this study are shown to be largely unbiased by relative 2-D and 3-D seismic data coverage. Contrary to expectation, the advantage of 3-D over 2-D seismic data for identifying site-specific targets appears to have been negligible.

Active fluid loss from depth in the Baram delta pseudo-accretionary prism is the prime factor influencing the distribution of heat flow and thermogenic surface hydrocarbons. Calculations support that bubble ascent and/or gas-phase migration may contribute significantly to the observed anomalous heat flow and surface hydrocarbons. Our data support greater flow conduit potential within the landward Baram delta than in the seaward half of our study area. Although the sources of fluids and the driving forces may have evolved, this flow occurs, possibly along preexisting faults, despite the absence of active subduction. Results are in accordance with global correlation between hydrocarbons and their thermal regimes in predicting enhanced generation, migration, and accumulation within the Baram delta sediments. Geothermal gradients from well data have previously been shown to be the most important factor influencing the distribution of oil and gas production in the region (Xia et al., 1995).

A simple diffusion model represents correlated heat flow and surface hydrocarbon data as being caused by near-surface processes, including migration, fractionation, mixing, and biodegradation within approximately 500 m (1640 ft) of lateral distance from seeps. However, more rapid vertical fluid flow from depth is required to explain the observed high (604 mW/m^2) heat flow and seep geochemistry and to effectively supply the line source in the diffusion model (Appendix 5). We cannot distinguish between seeped hydrocarbons that are the result of secondary migration directly from source rocks or tertiary migration from reservoirs. Active fluid flow and hydrothermal convection indicated by heat flow (e.g., over midocean ridges) are not necessarily associated with seeped hydrocarbons; nor are

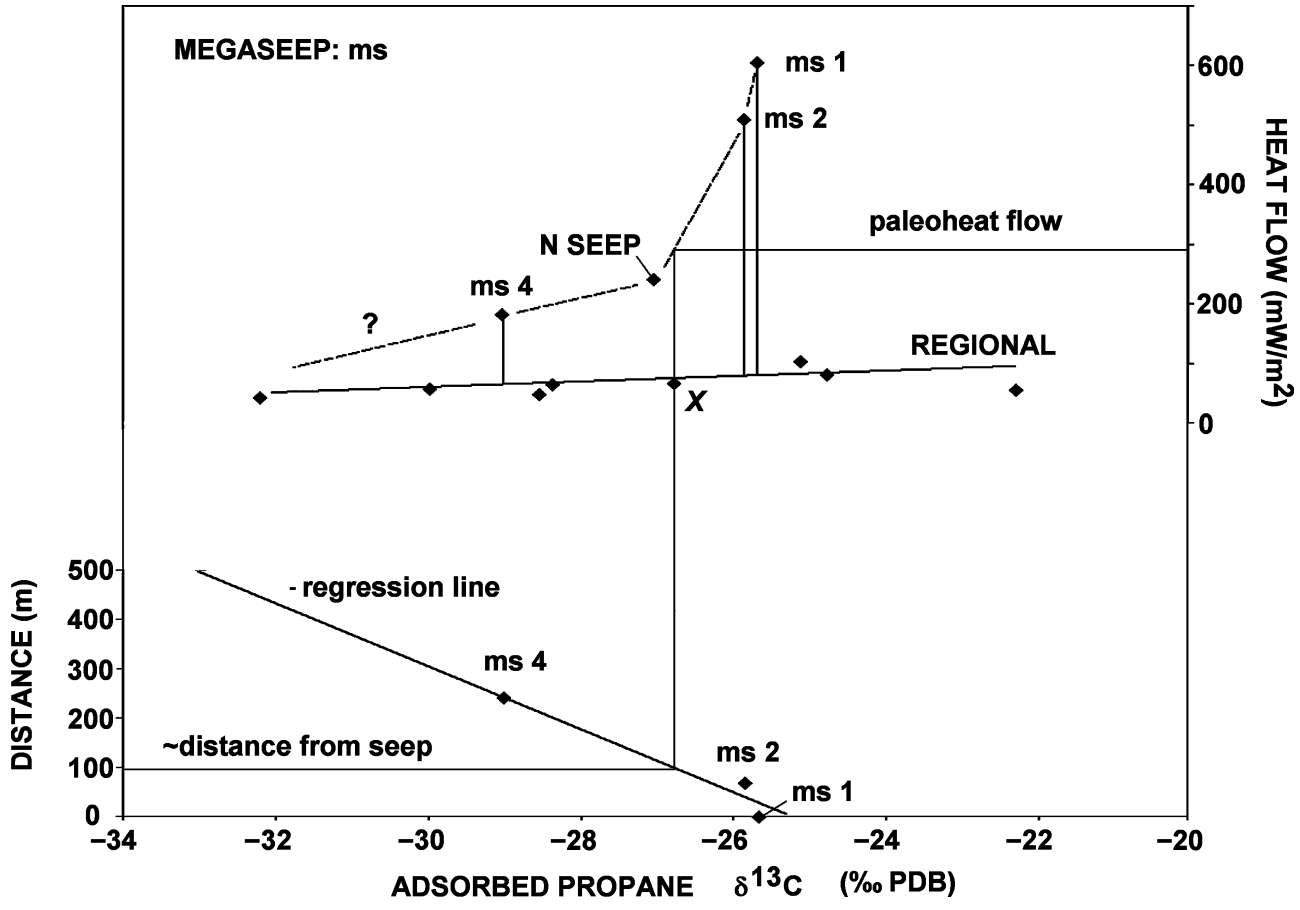

Figure 20. Hypothetical evolution of category 2 parameters (e.g., Figures 9–12), whereby megaseep data (MS) decline in heat flow with time (vertical lines), with negligible change in chemistry (e.g., $\delta^{13}C_3$), reflecting the origin of regional data (upper plot, heat flow versus geochemistry). Below, megaseep geochemistry versus distance from axis (from Figure 15) is plotted with the data (MS) regression line. This illustrates hypothetical derivation of paleoheat flow (upper plot) and distance from seep epicenter for an arbitrary regional data point (*X*). Scatter in regional heat flow (about regional line) may reflect different ages and amounts of thermal decline.

salt domes necessarily associated with hydrocarbons. However, in some petroliferous regions like the Gulf of Mexico, the salt dome–hydrocarbon association is well known. The degree of heat flow–hydrocarbon association shown in this study awaits testing in other petroliferous regions.

Operationally, results support the use of the Ewing technique for maximum heat-flow data sampling in combination with hydrocarbon geochemistry from 4-m (13-ft) site-specific gravity coring. Data dynamic range and coherency do not support a need for greater sediment penetration, which is operationally more problematic to consistently achieve. Results predict that for similar convective regimes, survey strategies that confine heat-flow measurements to the thermally uniform interiors of sediment troughs seriously underestimate mean regional heat flow (23–80%) and calculated hydrocarbon maturation and generation. Heat flow at all geochemical coring sites results in more reliable means and provides for real-time detection of active seeps. It draws attention to specific geochemical parameters that may more effectively reflect active seepage.

APPENDIX 1: SAMPLING AND MEASUREMENTS

Heat-flow measurements were obtained via the Ewing technique (Langseth, 1965), with six thermistors attached to a 4-m (13-ft) gravity corer barrel. Thermistor outputs were monitored and stored in situ. Less than 5 min of equilibration time were required to obtain thermal gradient (*G*) measurements at each site. At the surface, each plastic-lined core was divided into sections for immediate geochemical sample storage and for needle-probe thermal conductivity (*k*) measurements (Von Herzen and Maxwell, 1959). For the latter, small holes were drilled in the sealed core sections for insertion of the needle probe into equilibrated sediment samples. A total of

909 measurements were corrected to seabed temperatures (Ratcliffe, 1960), averaged, and combined with gradient data to obtain heat-flow values for each site ($HF = -kG$). Overall, we estimate the error of individual heat-flow measurements at less than 5%.

Core samples for geochemistry were canned, flushed with nitrogen, sealed, and immediately frozen to −80°C to avoid biological activity. Live oil, collected in sample bottles, and all sediment samples, packed in special containers with dry ice, were transported to our laboratory for analyses. These analyses included headspace gas, occluded gas, adsorbed gas, solvent extraction, quantitative gas chromatography of extracts, TSF of the extract, total organic carbon, and total carbon for all samples. High-resolution gas chromatography–mass spectrometry (GC-MS) of the extracts (EOM) that contained thermogenic hydrocarbons, and gas chromatography–isotope ratio mass spectrometry (compound-specific isotope analysis) of the gas fractions that contained thermogenic gases were also performed. Identification of EOM with abundant thermogenic hydrocarbons is based on chromatograms exhibiting abundant n-alkanes with low carbon preference indices (CPI) and typical oil profiles, with or without broad unresolved envelopes. Sample chromatograms are shown in Figure 21. Identification of thermogenic gases is by a combination of several parameters, including high values of wetness, abundant branched and cyclic compounds, and low alkenes (e.g., Hunt, 1979; Waples, 1981).

Compared with gravity coring, heat-flow measurements performed in conjunction with piston coring are more disturbed because of the rapid entry into the sediments (Davis, 1988). The use of gravity coring with 4-m (13-ft) core barrels for this survey routinely resulted in either full vertical penetration of the sediment or no penetration when submarine reefs were occasionally struck. When the latter occurred, locations were adjusted until full penetration was achieved. With full penetration, all thermistors entered the sediment, and the depth of geochemical sampling was relatively uniform.

APPENDIX 2: SEMIELLIPTICAL TROUGH MODEL

According to Lachenbruch and Marshall (1966), the heat flow inside a semielliptical sedimentary trough (HF_i) is given by $HF_i = K \times HF_m \frac{D+1}{D+K}$, where $K = 10$ is the ratio of thermal conductivity inside to outside (Figure 6); HF_m is the mean regional heat flow; and $D = d/hw$ is the ratio of the cylinder's vertical to horizontal semiaxes, i.e., the trough's depth (d)–to–half-width (hw) ratio. At the contact (outside the sediment trough), the heat flow (HF_o) is given by $HF_o = HF_m \frac{D+1}{D+K}$. The discontinuity in heat flow across the contact $HF_i/HF_o = K$.

APPENDIX 3: CALCULATION OF FLOW RATE

Blanche and Blanche (1997) report the average geothermal gradient (G) for the Sarawak shelf at 4.35°C/100 m (43.5°C/km) based on data from Rutherford and Qureshi (1981). Using the mean heat flow of 77.6 mW/m^2 obtained for our study area, we arrive at a value for

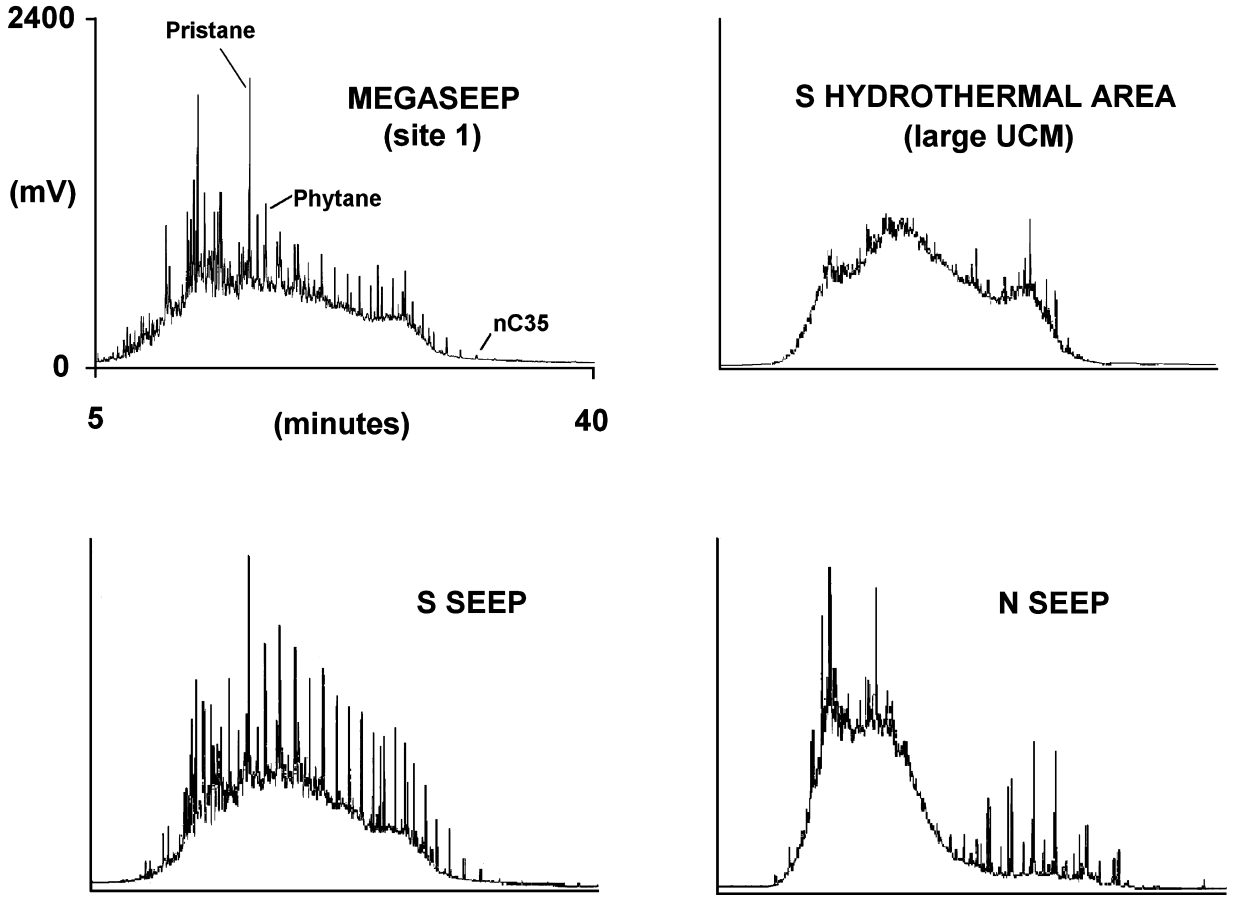

Figure 21. Sample chromatograms for hydrocarbon seeps located in Figure 4.

thermal conductivity (HF/G) of 1.78 W/m/K. This value (4.26×10^{-3} cal/cm/K) agrees with measured values (Clark, 1966; Kappelmeyer and Haenel, 1974) for various basin sediments comprising the northern Borneo margin (Blanche and Blanche, 1997).

Bredehoeft and Papadopulos (1965) quantify the effect of vertical water flow from depth ($z = L$) to the surface on a simple linear geotherm. For $\beta = \frac{1}{k}(\rho_w c_w \nu_z L)$, where k is thermal conductivity and ρ_w, c_w, and ν_z are the density, heat capacity, and vertical flow velocity of water, respectively, Zielinski and Bruchhausen (1983) showed that surface heat flow is altered because of vertical water flow by the factor $\frac{\beta}{e^{\beta}-1}$. For the megaseep, this has a value of 7.7, the ratio of the megaseep heat flow (604 mW/m^2) to the regional mean heat flow (77.6 mW/m^2). From β, we calculate $\nu_z = -5.5 \times 10^{-10}$ m/s (1.80×10^{-11} ft/s) (-1.7 cm/yr; 0.67 in./yr), the upward velocity required to account for the megaseep heat-flow anomaly by vertical water flow (L = 6000 m [19,685 ft], k = 1.78 W/m/K, and $\rho_w c_w = 4.186 \times 10^6$ J/m^3/K) (1 W = 1 J/s). In the case of gas-phase flow for density ρ_g = 0.1 g/cm^3 (Brown, 2000) and from heat capacity data (e.g., table 5-2 in Zemansky, 1968), we estimate $\rho_g c_g = 0.1 \times 10^6$ J/m^3 and $\rho_w c_w / \rho_g c_g$ = 42. Hence, to account for the megaseep anomaly under the same model conditions but for gas-phase flow, $\nu_{zg} = 42\nu_{zw}$ and $\nu_{zg} = -2.3 \times 10^{-8}$ m/s (-7.5×10^{-8} ft/s) (-72.5 cm/yr; -28.5 in./yr).

APPENDIX 4: CROSSPLOTS

To further investigate possible correlations between heat flow and geochemistry, we generated 181 crossplots of heat flow and nearly all geochemical parameters representing C_1 to C_{35} hydrocarbons and their ratios from analyses of headspace gas, occluded gas, adsorbed gas, EOM hydrocarbons, including GC-MS, carbon isotope, biomarker, and fluorescence (TSF) data. The geochemical parameters represent a full spectrum of data obtainable in surface geochemical coring programs. Crossplots were generated from all data collected, without regard to expectations based on prior data reports. Representative samples of these are shown in Figures 7–14. Except for isotopic data, we have not included methane results in Figures 7–14 because of the likelihood of significant biogenic contribution. Headspace gases were found anomalous only at the maximum heat flow (604 mW/m^2) megaseep site 1 (Figure 15). Hence, their contribution to the data interpretation presented is limited. Occluded gas and adsorbed gas hydrocarbon results were found to be in good agreement. The crossplots allow comparison of seep data (N, S, and megaseep) magnitudes with those for the entire data set.

APPENDIX 5: DIFFUSION MODEL

The theoretical results in Figure 17 (D = 157 m [515 ft]) are derived from a thermal diffusion model, where surface heat flow (HF) resulting from a line source of heat (Q) generated per unit length per unit time at depth $z = D$ is (Von Herzen and Uyeda, 1963)

$$\mathrm{HF} = \left(\frac{Q}{\pi}\right)\frac{\frac{1}{D}}{1+\frac{x^2}{D^2}}$$

The heat flow directly over the line source ($\mathrm{HF_o}$) at $x = 0$ is given by ($\mathrm{HF_o} = \frac{Q}{\pi}\frac{1}{D}$, and the relative heat flow is)

$$\frac{\mathrm{HF}}{\mathrm{HF_o}} = \left[1+\frac{x^2}{D^2}\right]^{-1}$$

.

Using this same model for the concentration ratios of the geochemical parameters, we substitute concentration (C) for temperature in equation 11 of Von Herzen and Uyeda (1963), and the relative concentration becomes

$$\frac{\mathrm{C}}{\mathrm{C_o}} = \frac{ln\ A}{ln\ B} \quad \text{where } A = \frac{x^2+(z-D)^2}{x^2+(z+D)^2} \quad \text{and } B = \frac{(z-D)^2}{(z+D)^2}$$

APPENDIX 6: THERMOGENIC MODEL

For a first-order quantitative assessment of any direct effect of heat flow on the surface distribution of geochemical parameters, we make use of the time-temperature index (TTI) of Lopatin (1971), as calibrated by Waples (1980), and defined by

$$\mathrm{TTI} = \int_0^{t'} 2^{\frac{T(t)-105}{10}} dt \qquad (1)$$

where T and t are temperature (°C) and time (m.y.), respectively. This equation approximates the alteration of organic matter as a kinetic process, whereby reaction rate doubles with every 10° rise in temperature. We have chosen to use this formulation as opposed to those based on the Arrhenius equation (e.g., Tissot and Welte, 1978) because temperature intuitively appears in the numerator of the exponent in equation 1 and for mathematical simplicity. We feel that the uncertainty associated with this approximation (e.g., Sweeney and Burnham, 1990) is small enough to justify this approach as a first approximation, with no computer necessary.

Accordingly, we use equation 1 to estimate the bulk effect of exposing organic material to a higher thermal regime brought about by a higher mean heat flow, for otherwise the same geohistory. In our simplified model, we assume

$$\mathrm{TTI} = 2^{\frac{T^*-105}{10}}\Delta t \qquad (2)$$

and

$$\frac{\mathrm{TTI}}{\mathrm{TTI_o}} = 2^{\frac{T^*-105}{10}} = \frac{\mathrm{C}}{\mathrm{C_o}} \quad (\Delta t \text{ constant}) \qquad (3)$$

where $\mathrm{TTI_o}$ represents the onset of alteration, when T = 105°C, resulting from an initial mean (constant) heat flow ($\mathrm{HF_o}$); T^* is a higher mean (constant) temperature resulting from higher mean (constant) heat flow (HF*), where

$$T^* = \frac{z}{k}\mathrm{HF}^* \qquad (4)$$

and

$$z = \frac{105k}{\mathrm{HF_o}} \qquad (5)$$

the depth where T = 105°C for the initial heat flow ($\mathrm{HF_o}$), and k is thermal conductivity, assumed constant. (Note that for z in meters and k in W/m/K, HF values are in W/m^2.) Equation 3 assumes that the TTI ratio reflects the extent of reaction resulting from the increased heat flow (HF*) and, hence, the concentration ratio ($\mathrm{C/C_o}$) of reaction products. Note that this concentration ratio is fundamentally

different from that for the diffusion model, where C_o (Appendix 5) corresponds to the highest heat flow.

Temperature values (T^*) were computed first from the simple (equation 4) conductive geotherm (COND), with k = 1.78 W/m/K estimated from the average geothermal gradient (G) reported for the Sarawak shelf (Rutherford and Qureshi, 1981; Blanche and Blanche, 1997) of 4.35°C/100 m (43.5°C/km), and the mean heat flow (HF_m) of 77.6 mW/m^2 obtained for our Brunei study area ($k = HF_m/G$).

We also calculate T^* for equation 3 not using the conductive equation 4, but by the simple convective model (CONV) of Bredehoeft and Papadopulos (1965). It quantifies the effect of vertical water flow (v_z) from depth ($z = L$) to the surface ($z = 0$) on a simple linear geotherm (T), where

$$\frac{T}{T_L} = \frac{e^{\frac{\beta z}{L}} - 1}{e^{\beta} - 1} = 1 - e^{\frac{\beta z}{L}} \quad (T = 0 \text{ at } z = 0,\ T = T_L \text{ and } e^{\beta} \to 0 \text{ at } z = L) \qquad (6)$$

$$\beta = \frac{\rho_w c_w v_z L}{k} \qquad (7)$$

and ρ_w, c_w, v_z, and k are the density, heat capacity, and vertical flow velocity of water respectively, and k is thermal conductivity. Vertical flow velocities upward have negative values ($v_z < 0$) as do values of β. Zielinski and Bruchhausen (1983) showed that surface heat flow is altered because of vertical water flow by the factor

$$\frac{\beta}{e^{\beta} - 1} \qquad (8)$$

For both models (COND and CONV), T_L = 261°C at L = 6000 m (19,685 ft). In CONV, for any initial heat-flow value (HF_o), a value of β (β_o) is calculated from expression 8 (L = 6000 m [19,685 ft], k = 1.78 W/m/K, and $\rho_w c_w$ = 4.186 J/m/K), and equation 6 is used to calculate z for T = 105°C. Then, for a higher heat flow (HF*), a new value of β (β*) is calculated from expression 8, and equation 6 is used to calculate $T = T^*$ using the initial value for z. Equation 3 is then used to compute relative concentrations (C/C_o).

REFERENCES CITED

Abrams, M. A., 1996a, Distribution of subsurface hydrocarbon seepage in near-surface marine sediments: Detection of surface hydrocarbons, *in* D. Schumacher and M. A. Abrams, eds., Hydrocarbon migration and its near-surface expression: AAPG Memoir 66, p. 1–14.

Abrams, M. A., 1996b, Interpretation of methane carbon isotopes extracted from surficial marine sediments for detection of surface hydrocarbons, *in* D. Schumacher and M. A. Abrams, eds., Hydrocarbon migration and its near-surface expression: AAPG Memoir 66, p. 309–318.

Anderson, R. N., 1980, 1980 update of heat flow in the east and southeast Asian seas, *in* D. E. Hayes, ed., The tectonic and geologic evolution of the southeast Asian seas and islands: Geophysical Monograph Series, v. 23, p. 319–326.

Barwise, T., and S. Hay, 1996, Predicting oil properties from core fluorescence, *in* D. Schumacher and M. A. Abrams, eds., Hydrocarbon migration and its near-surface expression: AAPG Memoir 66, p. 363–371.

Bernard, B. B., J. M. Brooks, and W. M. Sackett, 1977, A geochemical model for characterization of hydrocarbon gas sources in marine sediments: Offshore Technology Conference, Houston, Texas, no. 2934, p. 435–438.

Bjørlykke, K., 1993, Fluid flow in sedimentary basins: Sedimentary Geology, v. 86, p. 137–158.

Bjørlykke, K., 1999, Principal aspects of compaction and fluid flow in mudstones, *in* A. C. Halpin, A. J. Fleet, and J. H. S. Macquaker, eds., Muds and mudstones: Physical and fluid flow properties: Geological Society (London) Special Publications, v. 158, p. 73–78.

Blanche, J. B., and J. D. Blanche, 1997, An overview of the hydrocarbon potential of the Spratly Island archipelago and its implications for regional development, *in* A. J. Fraser, S. J. Matthews, and R. W. Murphy, eds., Petroleum geology of southeast Asia: Geological Society (London) Special Publication 126, p. 293–310.

Bredehoeft, J. D., and I. S. Papadopulos, 1965, Rates of vertical groundwater movement estimated from the Earth's thermal profile: Water Resources Research, v. 1, p. 325–328.

Brooks, J. M., B. B. Bernard, W. M. Sackett, and J. R. Schwarz, 1979, Natural gas seepage on the south Texas shelf: Offshore Technology Conference, Houston, Texas, no. 3411, p. 471–478.

Brooks, J. M., M. C. Kennicut, L. A. Barnard, G. J. Denoux, and B. D. Carey, 1983, Application of total scanning fluorescence to exploration geochemistry: Offshore Technology Conference, Houston, Texas, no. 4624, p. 393–400.

Brooks, J. M., M. C. Kennicut, and B. D. Carey, Jr., 1986, Offshore surface geochemical exploration: Oil & Gas Journal, v. 84 (October 20, 1986), p. 66–72.

Brown, A., 2000, Evaluation of possible gas microseepage mechanisms: AAPG Bulletin, v. 84, p. 1775–1789.

Carslaw, H. S., and J. C. Jaeger, 1959, Conduction of heat in solids: Oxford, United Kingdom, Clarendon Press, 510 p.

Clark, S. P. Jr., 1966, Thermal conductivity, *in* S. P. Clark, Jr., ed., Handbook of physical constants: Geological Society of America Memoir 97, p. 459–482.

Davis, E. E., 1988, Oceanic heat-flow density, *in* R. Haenel, L. Rybach, and L. Stegena, eds., Handbook of terrestrial heat-flow density determination: Dordrecht, Kluwer Academic Publishers, p. 223–260.

Davis, E. E., R. D. Hyndman, and H. Villinger, 1990, Rates of fluid expulsion across the northern Cascadia accretionary prism: Constraints from new heat flow and multichannel seismic data: Journal of Geophysical Research, v. 95, p. 8869–8889.

Davis, J. C., 1986, Statistics and data analysis in geology, 2d ed.: New York, New York, John Wiley & Sons, 646 p.

Fisher, A. T., and M. W. Hounslow, 1990, Transient fluid flow through the tow of the Barbados accretionary complex: Constraints from Ocean Drilling Program Leg 110 heat flow studies and simple models: Journal of Geophysical Research, v. 95, p. 8845–8858.

Fisher, Q. J., M. Casey, S. D. Harris, and R. J. Knipe, 2003, Fluid-flow properties of faults in sandstone: The importance of temperature history: Geology, v. 31, p. 965–968.

Fowler, P. T., 1980, Telling live basins from dead ones by temperature: World Oil, May, p. 107–122.

Furukawa, Y., 1995, Temperature structure in the crust of the Japan arc and the thermal effects of subduction, *in* M. L. Gupta and M. Yamano, eds., Terrestrial heat flow and geothermal energy in Asia: Rotterdam, A. A. Balkema, p. 203–219.

Hunt, J. M., 1979, Petroleum geochemistry and geology: San Francisco, California, W. H. Freeman and Company, 617 p.

Hutchison, C. S., 2005, Geology of north-west Borneo: Sarawak, Brunei and Sabah: Amsterdam, Netherlands, Elsevier, 421 p.

Jones, V. T., and R. J. Drozd, 1983, Predictions of oil or gas potential

by near potential by near-surface geochemistry: AAPG Bulletin, v. 67, p. 932–952.
Kappelmeyer, O., and R. Haenel, 1974, Geothermics with special reference to application: Berlin, Gebruder Borntraeger, Geoexploration Monographs, series 1, no. 4, 238 p.
Klaucke, I., H. Sahling, D. Burk, W. Weinrebe, and G. Bohrmann, 2005, Mapping deepwater gas with sidescan sonar: EOS Transactions of the Americal Geophysical Union, v. 86, p. 341.
Klemme, H. D., 1975, Geothermal gradients, heat flow, and hydrocarbon recovery, *in* A. Fischer and S. Judson, eds., Petroleum and global tectonics: Princeton, New Jersey, Princeton University Press, p. 251–304.
Lachenbruch, A. H., and B. V. Marshall, 1966, Heat flow through the Arctic Ocean floor: The Canada basin–alpha rise boundary: Journal of Geophysical Research, v. 71, p. 1223–1248.
Langseth, M. G., 1965, Techniques of measuring heat flow through the ocean floor, *in* W. Lee, ed., Terrestrial heat flow: American Geophysical Union Monograph Series, no. 8, p. 58–77.
Langseth, M. G., and J. C. Moore, 1990, Introduction to the special section on the role of fluids in sediment accretion, deformation, diagenesis, and metamorphism in subduction zones: Journal of Geophysical Research, v. 95, p. 8737–8741.
Langseth, M. G., and E. A. Silver, 1996, The Nicoya convergent margin— A region of exceptionally low heat flow: Geophysical Research Letters, v. 23, p. 891–894.
Langseth, M. G., G. K. Westbrook, and M. Hobart, 1990, Contrasting geothermal regimes of the Barbados ridge accretionary complex: Journal of Geophysical Research, v. 95, p. 8829–8843.
Lee, W. H. K., 1970, On the global variations of terrestrial heat flow: Physics of the Earth and Planetary Interiors, v. 2, p. 332–341.
Lee, W. H. K., and S. Uyeda, 1965, Review of heat flow data, *in* W. H. K. Lee, ed., Terrestrial heat flow: Geophysical Monograph Series, no. 8, p. 87–190.
Lerche, I., 1990, Basin analysis: Quantitative methods: San Diego, Academic Press, 570 p.
Letouzey, J., L. Sage, and C. Muller, 1988, Geological and structural map of eastern Asia: AAPG, scale 1:2,500,000, 3 sheets.
Lopatin, N. V., 1971, Temperature and geologic time as factors in coalification (in Russian): Izvestiia Akademii Nauk, SSSR, Seriya Geologischeswkaya, no. 3, p. 95–106.
MacKenzie, A. S., and D. McKenzie, 1983, Isomerization and aromatization of hydrocarbons in sedimentary basins formed by extension: Geology Magazine, v. 120, p. 417–470.
Mason, E. A., and R. B. Evans, 1969, Graham's laws: Simple demonstrations of gases in motion: Journal of Chemical Education, v. 46, p. 358–364.
Mason, E. A., and T. R. Marrero, 1970, The diffusion of atoms and molecules: Advances in Atomic and Molecular Physics, v. 6, p. 155–232.
Mat-Zin, I. C., and R. E. Swarbrick, 1997, The tectonic evolution and associated sedimentation history of Sarawak Basin, eastern Malaysia: A guide for future hydrocarbon exploration, *in* A. J. Frazer, S. J. Matthews, and R. W. Murphy, eds., Petroleum geology of southeast Asia: Geological Society (London) Special Publication 126, p. 237–245.
Moldowan, J. M., P. Sundararaman, and M. Schoell, 1986, Sensitivity of biomarker properties to depositional environment and/or source input in the Lower Toarcian of S. W. Germany: Organic Geochemistry, v. 10, p. 915–926.
Nagihara, S., J. M. Brooks, B. B. Bernard, N. Summer, G. Cole, and T. Lewis, 2002, Application of marine heat flow important in oil, gas exploration: Oil and Gas Journal, v. 100.27 (July 8, 2002), p. 43–49.
Parsons, B., and J. G. Sclater, 1977, An analysis of the variation of ocean floor bathymetry and heat flow with age: Journal of Geophysical Research, v. 82, p. 803–827.
Peters, K. E., C. C. Walters, and J. M. Moldowan, 2005, The biomarker guide: Interpreting molecular fossils in petroleum exploration and Earth history: Cambridge, United Kingdom, Cambridge University Press, v. 2, p. 475–1155.
Pollack, H. N., S. J. Hurter, and J. R. Johnson, 1993, Heat flow from the Earth's interior: Analysis of the global data set: Reviews of Geophysics, v. 31, p. 267–280.
Radke, M., 1987, Organic chemistry of aromatic hydrocarbons, *in* J. Brooks and D. Welte, eds., Advances in petroleum geochemistry: London, Academic Press, v. 2, p. 141–207.
Radke, M., and D. H. Welte, 1983, The methylphenanthrene index (MPI): A maturity parameter based on aromatic hydrocarbons, *in* M. Bjorøy, P. Albrecht, C. Cornford, K. de Groot, G. Eglinton, E. Galimov, D. Leythaeuser, R. Pelet, J. Rulkotter, and G. Speers, eds., Advances in organic geochemistry 1981: New York, John Wiley & Sons, p. 504–512.
Radke, M., D. H. Welte, and H. Willsch, 1982, Geochemical study on a well in Western Canada basin: Relation of the aromatic distribution pattern to maturity of organic matter: Geochimica et Cosmochimica Acta, v. 46, p. 1–10.
Rashid, M. A., and J. D. McAlary, 1977, Early maturation of organic matter and genesis of hydrocarbons as a result of heat from a shallow piercement salt dome: Journal of Geochemical Exploration, v. 8, p. 549–569.
Ratcliffe, E. H., 1960, The thermal conductivities of ocean sediments: Journal of Geophysical Research, v. 65, p. 1535–1541.
Ritter, U., G. W. Zielinski, H. M. Weiss, R. L. B. Zielinski, and J. Saettem, 2004, Heat flow in the Vøring Basin, mid-Norwegian shelf: Petroleum Geoscience, v. 10, p. 353–365.
Roberts, W. H. III, 1981, Some uses of temperature data in petroleum exploration, *in* B. M. Gottlieb, ed., Unconventional methods in exploration for petroleum and natural gas: Dallas, Southern Methodist University Press, p. 8–49.
Ru, K., and J. D. Pigott, 1986, Episodic rifting and subsidence in the South China Sea: AAPG Bulletin, v. 70, p. 1136–1155.
Ruppel, C., and M. Kinoshita, 2000, Fluid, methane, and energy flux in an active margin gas hydrate province, offshore Costa Rica: Earth and Planetary Science Letters, v. 179, p. 153–165.
Ruppel, C., G. R. Dickens, D. G. Castellini, W. Gilhooly, and D. Lizarralde, 2005, Heat and salt inhibition in the northern Gulf of Mexico: Geophysical Research Letters, v. 32, no. L04605, p. 1–4.
Rutherford, K. J., and M. K. Qureshi, 1981, Geothermal gradient map of southeast Asia: Southeast Asia Petroleum Exploration Society and Indonesia Petroleum Association, 51 p.
Sassen, R., A. V. Milkov, H. H. Roberts, S. T. Sweet, and D. A. DeFreitas, 2003, Geochemical evidence of rapid hydrocarbon venting from a seafloor-piercing mud diapir, Gulf of Mexico continental shelf: Marine Geology, v. 198, p. 319–329.
Sassen, R., S. T. Sweet, D. A. DeFritas, N. L. Eaker, H. H. Roberts, and C. L. Zhang, 2004, Brine vents on the Gulf of Mexico slope: Hydrocarbons, carbonate-barite-uranium mineralization, red beds, and life in an extreme environment, *in* Salt-sediment interactions and hydrocarbon prospectivity: Concepts, applications, and case studies for the 21st century: 24th Annual Meeting Gulf Coast Section SEPM Research Foundation, p. 444–463.
Schumacher, D., and M. A. Abrams, eds., 1996, Hydrocarbon migration and its near-surface expression: AAPG Memoir 66, 450 p.
Sclater, J. G., J. Crow, and R. N. Anderson, 1976, On the reliability of oceanic heat flow averages: Journal of Geophysical Research, v. 81, p. 2997–3006.
Screaton, E. J., D. R. Wunderlich, and S. J. Dreiss, 1990, Permeabilities, fluid pressures, and flow rates in the Barbados ridge complex: Journal of Geophysical Research, v. 95, p. 8997–9007.
Simoneit, B. R. T., and P. F. Lonsdale, 1982, Hydrothermal petroleum

in mineralized mounds at the seabed of the Guaymas Basin: Nature, v. 295, p. 198–202.
Sweeney, J. J., and A. K. Burnham, 1990, Evaluation of a simple model of vitrinite reflectance based on chemical kinetics: AAPG Bulletin, v. 74, p. 1559–1570.
Taylor, B., and D. E. Hayes, 1983, Origin and history of the South China Sea Basin, *in* D. E. Hayes, ed., The tectonic and geological evolution of the south east Asian seas and islands, part II: American Geophysical Union Geophysical Monograph Series, v. 27, p. 23–56.
Tissot, B., and J. Espitalie, 1975, L'evolution thermique de la matierer organique des sediments: Applications d'une simulation mathematique: Revue de l'Institut Français du Pétrole, v. 30, p. 743–777.
Tissot, B., and D. Welte, 1978, Petroleum formation and occurrence: Berlin, Springer-Verlag, 538 p.
Von Herzen, R. P., and A. E. Maxwell, 1959, The measurement of thermal conductivity of deep-sea sediments by a needle probe method: Journal of Geophysical Research, v. 64, p. 1557–1563.
Von Herzen, R. P., and S. Uyeda, 1963, Heat flow through the Pacific Ocean floor: Journal of Geophysical Research, v. 68, p. 4219–4250.
Vrolijk, P., A. Fisher, and J. Gieskes, 1991, Geochemical and geothermal evidence for fluid migration in the Barbados accretionary prism (ODP leg 110): Geophysical Research Letters, v. 18, p. 947–950.
Waples, D., 1981, Organic geochemistry for exploration geologists: Minneapolis, Burgess Publishing Co., 151 p.
Waples, D. W., 1980, Time and temperature in petroleum exploration: AAPG Bulletin, v. 64, p. 916–926.
Watanabe, T., M. G. Langseth, and R. N. Anderson, 1977, Heat flow in back-arc basins of the western Pacific, *in* M. Talwani and W. C. Pitman, III, eds., Island arcs, deep sea trenches, and back-arc basins: Maurice Ewing Series 1, American Geophysical Union, p. 137–161.
Williams, D. L., R. P. Von Herzen, J. G. Sclater, and R. N. Anderson, 1974, The Galapagos spreading center: Lithospheric cooling and hydrothermal circulation: Geophysical Journal of the Royal Astronomical Society, v. 38, p. 587–608.
Xia, K., S. Xia, Z. Chen, and C. Huang, 1995, Geothermal characteristics of the South China Sea, *in* M. L. Gupta and M. Yamano, eds., Terrestrial heat flow and geothermal energy in Asia: Rotterdam, A. A. Balkema, p. 113–128.
Yoshii, T., Y. Kono, and K. Ito, 1976, Thickening of the oceanic lithosphere, *in* G. P. Woolard, G. H. Sutton, M. H. Manghnani, and R. Moberly, eds., The geophysics of the Pacific Ocean basin and its margin: American Geophysical Union Monograph Series, v. 19, p. 423–430.
Zemansky, M. W., 1968, Heat and thermodynamics: New York, New York, McGraw-Hill Book Co., p. 124.
Zielinski, G. W., 1977, Thermal evolution of the Norwegian-Greenland Sea and its rifted continental margin: Ph.D. thesis, Columbia University, New York, New York, 161 p.
Zielinski, G. W., 1979, On the thermal evolution of passive continental margins, thermal depth anomalies, and the Norwegian-Greenland Sea: Journal of Geophysical Research, v. 84, p. 7577–7588.
Zielinski, G. W., and P. M. Bruchhausen, 1983, Shallow temperatures and thermal regime in the hydrocarbon province of Tierra del Fuego: AAPG Bulletin, v. 67, p. 166–177.
Zielinski, G. W., J. A. Drahovzal, G. M. DeCoursey, and J. M. Ruperto, 1985, Hydrothermics in the Wyoming overthrust belt: AAPG Bulletin, v. 69, p. 699–709.
Zielinski, G. W., F. J. Nassauer, R. L. B. Zielinski, M. G. Lindgren, and U. S. Raetz, 1990, Heat flow measurements in early exploration strategy: Geological Journal of the Ukrainian Academy of Science, v. 1, p. 33–39.
Zielinski, G. W., M. Bjorøy, and R. L. B. Zielinski, 2003, Heat flow and surface geochemistry on the Brunei continental margin (abs.): AAPG Annual Convention Program, v. 12, p. A189.